Synthesis and additive manufacturing of titanium carbide ($Ti_3C_2T_x$) *MXene* electrochemical sensors for nitrophenols

by

Shiseido Robinson

B.S., Kansas State University, 2021

A THESIS

submitted in partial fulfillment of the requirements for the degree

MASTER OF SCIENCE

Department of Industrial and Manufacturing Systems Engineering
Carl R. Ice College of Engineering

KANSAS STATE UNIVERSITY
Manhattan, Kansas

2023

Approved by:

Major Professor
Suprem R. Das

Copyright

Abstract

The discovery of two-dimensional transition metal carbides and carbonitrides (*MXene*) has laid the foundation for further investigations in layered materials for its superior performance and applications. The material embodies countless desired properties such as hydrophilic surfaces, high electrical and thermal conductivities, large surface-to-volume ratio, excellent mechanical robustness, and efficient absorption of electromagnetic waves. The unique properties of these easily processable 2D layered *MXene* materials have been explored largely in energy storage devices and electromagnetic shielding applications for almost a decade. More recently, the material has attracted enormous interest in the field of chemical and biomolecule sensing owing to its varied chemical structure and ease of functionalization for sensitive and selective detection of various analytes. In this thesis, the large-scale exfoliation of the widely studied $Ti_3C_2T_x$ *MXene* materials by adopting a minimally intensive layer delamination (MILD) etching route is demonstrated. Controlled chemical exfoliation conditions lead to the selective removal of the Al layer from Ti_3AlC_2 to form a few layered *MXene*. Subsequently, the exfoliated *MXene* clay was collected and re-dispersed in water and concentrated to form additive-free stable conductive inks. The ideal synthesis conditions for successful etching of *MXene* material were confirmed and examined through different structural and morphological characterizations such as X-ray diffraction (XRD), scanning electron microscope (SEM), transmission electron microscopy (TEM), X-ray photoelectron spectroscopy (XPS), Raman spectroscopy, and atomic force microscopy (AFM). Successfully synthesized *MXene* inks were used for dispense printing to fabricate sensor electrodes. The electrochemical performance of pure *MXene* and printed *MXene*

electrodes were analyzed with a standard redox probe and its sensing behavior towards quantification of 4-Nitrophenol was examined.

Table of Contents

List of Figures

List of Tables

Chapter 1 - Introduction

1.1 Nanomaterials

The development of nanotechnology has revolutionized the impact of natural sciences and engineering. Nanotechnology deals in the development and application of nanomaterials based on fundamental scientific knowledge obtained from nanoscience. It deals with materials where some controllable relevant dimension is of the order of 100 nm or less [1]. There are three different classes of nanomaterials: discrete nanomaterials, nanoscale device materials, and bulk materials. Discrete nanomaterials or dn materials are material elements that are freestanding and 1–10 nm in scale in at least one dimension some include nanoparticles and nanofibers such as carbon nanotubes. Nanoscale device materials or nd materials are nanoscale material elements that are contained within devices, usually as thin films. An example of a nd material is a thin film of metal oxide that is used within some semiconductor fabrication [1].

Table 1. A broad classification of nanomaterials based on dimensionality and morphology.

Type of nanomaterial	Dimensionality	Morphology	Characteristics	Remarks
Discrete nano (dn) materials	0D or 1D	Particles, fibers	Large surface functionalization	Potential health hazard
Nanoscale device (nd) materials	Usually 2D, occasionally 1D	Thin films, sometimes wires	Functionalization, electrical/thermal characteristics	Semiconductor fabrication
Bulk (nc or ns) nanomaterials	3D	Minimum mm3	Mechanical and structural applications	May be built up from dn and nd materials

Nanomaterials are synthesized through two major approaches, one is top-down where a bulk material is tailored down to the nanoscale dimension by employing certain processes and the other is a bottom-up approach, where small molecules are combined to produce nanomaterials by certain processes. Nanomaterials undergo several synthesis methods that are either chemical, physical, mechanical, or biological. Nanomaterials display a high surface/volume ratio, which

offers good performance that can be applied in many nanotechnology applications such as nanosensors and renewable energy devices. Furthermore, nanomaterials have shown higher adsorption capacity in both gas and liquid phases [2]. Other properties like physical, chemical, morphological, mechanical, thermal, optical, magnetic, and conductivity come through the selection, doping, and composition of different materials. Many have exploited the inherent, modified, and added characteristics of these nanomaterials to several fields like energy, medicine, environmental science, information technology, homeland security, food safety, and transportation [3]. Some well-known nanomaterials include graphene-based nanomaterials, metal-organic frameworks, carbon nanotubes and their composites, nanostructured thin films, conducting polymers and their composites, *MXene*s, chalcogenide nanocrystals, and quantum dots [4], [5].

1.2 Zero Dimensional (0D) to Two-Dimensional (2D) materials

For the past 19 years, starting with the discovery of single-layer and few layer graphene with its unique physical properties, two-dimensional (2D) materials have been widely researched. Graphene, mechanically exfoliated from graphite was discovered in 2004 and has been extensively studied in the scientific world due to the materials' large surface area, high thermal conductivity, high electron mobility, strong chemical durability, and excellent mechanical stability [6]. This groundbreaking discovery led to studies on the synthesis and characterizations of high-quality 2D materials beyond graphene. For instance, transition metal dichalcogenides (TMDs) and oxides (TMOs), silicene, germanene, borophene, etc., are all fascinating 2D materials that add a large diversity of unique properties to this 2D family, which is still expanding rapidly [7]. Transition metal carbides, carbonitrides, and nitrides, known as *MXene*s, are a new class of 2D materials that have attracted ever-increasing research attention in many aspects and are standing at the frontier

of the 2D materials community, especially for their metallic type of behavior but more and more other electronic type are being explored [8],[9].

1.3 MXene and its structure

The interest in exploring graphene and thinning down the thickness of three-dimensional materials to 2D atomically thin sheets has led to the discovery of many new 2D materials, one being *MXene* [6]. The first *MXene* ($Ti_3C_2T_x$) was discovered at Drexel University in 2011 [10]. *MXene* is an emerging class of 2D materials with a general formula $M_{n+1}X_nT_x$, where n = 1, 2, or 3; M refers to an early transition metal element; X represents carbon or nitrogen; and T corresponds to the surface terminations [6]. *MXene*s are obtained by selective etching of the A-element from the MAX (Ti_3AlC_2) phase, which leads to the resulting 2D transition metal carbides or nitrides. Figure 1 exhibits atomic schematics of three types of *MXene*s. The variety of compositions and structures of *MXene*s has led to the formation of a large and rapidly expanding family of 2D materials. *MXene*s were synthesized in 2014 and reported in 2015 and many new compositions have been synthesized in this subfamily of *MXene*s [13]. Synthesizing newly ordered two-dimensional carbide phases has raised much excitement in the MAX phase research community. Researchers who have been studying MAX phases for the past two decades began developing new *MXene* precursors. For instance, MAX phases but also other layered carbides and nitrides. Since 2017, more than 50 newly ordered double-transition metal MAX phases have been explored and their properties, including their magnetic characteristics [11]. Furthermore, computational studies on *MXene*s and their precursors have predicted more than hundreds of possible compositions [12], due to the formation of solid solutions on M and/or X sites offers possibilities for the synthesis of an infinite number of nonstoichiometric *MXene*s and the opportunity to finely tune properties by mixing different transition metals or creating carbonitrides. Hence, another advanced development

was the processes for fluoride-free synthesis of *MXene*s. In 2019, Huang et al. used molten $ZnCl_2$ salt to synthesize new MAX phases as well as fluorine-free *MXene*s [13]. Huang's method significantly has widened experimental research on *MXene*s where researchers can create *MXene*s but do not want to work with any hydrofluoric acid (HF)-containing or HF-forming chemicals in laboratories [14].

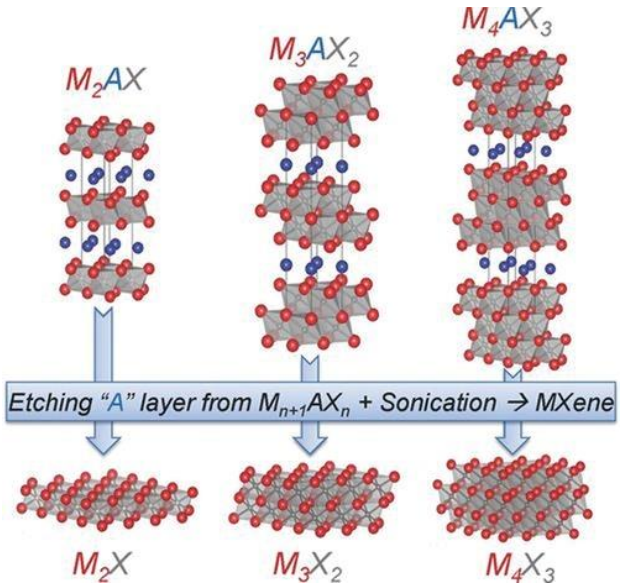

Figure 1: Structure of MAX phases and the corresponding *MXene*s derived from MAX. (reproduced by permission from Ref [32])

1.4 Properties of *MXene*

*MXene*s possess various unique properties. For instance, *MXene* exhibits high electrical conductivity and mechanical properties of transition metal carbides/nitrides; functionalized surfaces that make *MXene*s hydrophilic making it ready to bond to various species; high negative zeta potential, enabling stable colloidal solutions in water and efficient absorption of electromagnetic waves [14].

1.4.1 Electrical Properties

*MXene*s are known for their outstanding metallic behavior with a well-fixed electron density near the Fermi level [15]. It has been reported that metallic *MXene*, $Ti_3C_2T_x$ films display higher electrical conductivity than any other 2D materials, including exfoliated graphene, metal sulfides/hydroxides, etc., [16]. For instance, titanium carbide exfoliated using HF an electrical conductivity of 6500 S cm $^{-1}$ and a high capacitance of 1500 F cm^{-3} [17]. However, recent studies reported that the *MXene*s' electrical conductivity is also morphology and method of exfoliation condition dependent. For instance, ultra-thin compact *MXene* films with highly aligned flakes show a very high electrical conductivity of up to 19325 S cm^{-1} [42]. Etching methods also affect the electrical conductivity of *MXene*s; a stronger etchant means higher defect density in the resultant *MXene* samples. HF-etched $Ti_3C_2T_x$ powders display moderate electrical conductivities (<1000 S cm^{-1}) [18].

1.4.2 Work Function

MXene's work functions can be adjusted by surface groups by controlling the Fermi level shift and electronic redistribution [19]. The work function of $Ti_3C_2T_x$ *MXene* can be shifted in the range of 3.9 - 4.0 eV, depending on the annealing temperature associated with the surface termination moieties [20]. Moreover, $Ti_3C_2T_x$ with a very low work function of 4.37 eV can form a good Schottky contact with n-Si by van der Waals forces at room temperature, or Schottky-barrier-free contacts will act as a transparent electrode where it will enable the separation and transport of photoinduced carriers in self- driven photodetectors [21].

1.4.3 Optical Properties

During the delamination of multilayered *MXene* into fewer layers when suspended in water a Tyndall effect occurs because of its uniform dispersion. From ultrathin films made of

delaminated flakes, it has been reported that a transmittance up to 97% can be achieved, corresponding to continuous coverage of single-layer *MXene* nanosheets [22]. Furthermore, this implies that monolayer *MXene* leads to ~3% loss in transmittance, which is like graphene that shows 2.3% loss per layer [22]. When considering the thickness of a monolayer *MXene*, which is four times thicker than graphene (1.5 nm vs 0.34 nm). *MXene* possesses higher optical transmittance and better optoelectronic properties compared to those of graphene [23].

1.4.4 Magnetic Properties

In comparison to the optical and electrical properties, the magnetic properties of *MXene*s are less investigated. Most of the predicted magnetic *MXene*s are based on magnetic transition metal elements (Cr, V, Mn, Fe, Co and Ni) or their mixtures, and forming solid-state solutions [7]. Ti_2C and Ti_2N *MXene*s are claimed to show a nearly half-metallic ferromagnetism, while Mn_2C monolayer shows an antiferromagnetism with a high Neel temperature of 720 K [24]. Moreover, bare *MXene*s have been reported to be ferromagnets; but solution etched *MXene*s are always terminated with functional groups. The first synthesis of magnetic susceptibilities ($x = 5.7 \sim 52 \times 10^{-6}$) of reduced $Ti_3C_2T_x$ are temperature independent as T >10 K, indicative of Pauli paramagnetic properties [25].

1.4.5 Oxidation Stability

Oxidation stability of *MXene*s especially in suspensions is a major concern. While oxidation can be used for some applications such as energy storage, sensing, and disposable electronics, it is usually avoided when the electrical conductivity is important [26]. For instance, the presence of pinholes and defects are generally formed during the synthesis and accelerates the oxidation of *MXene*s, which then shortens their shelf life. This is due to water and dissolved oxygen playing the main role in the oxidation of *MXene*s. To prevent and minimize oxidation, proper

handling and storage of *MXene* aqueous dispersion in Ar-filled vials and low temperature (<5 °C) can prolong *MXene* shelf life [27]. Furthermore, it has been reported that freezing aqueous dispersions under –20 °C are reported to be capable of preserving the *MXene* flakes for up to two years [27]. Defects density and flake size highlight a strong relationship with controlling the oxidation kinetics. For instance, higher density of defects and smaller flake size will speed up the oxidation of *MXene* dispersions. Therefore, dispersing *MXene* nanosheets in non-aqueous polar solvents, such as NMP, DMSO, ethanol, etc., can minimize their interaction with water or dissolved oxygen to extend their shelf life [28]. Potential good solvents are those possessing a high surface tension, high boiling point, and a high dielectric constant, which can stabilize *MXene* nanosheets. Improving the oxidation stability by transferring to non-aqueous solvent is in more interest in solution processing of *MXene*s since in many of the deposition techniques [28].

1.5 Applications

*MXene*s have a unique combination of properties such as high electrical conductivity and mechanical properties of transition metal carbides/nitrides; functionalized surfaces that make *MXene*s hydrophilic and ready to bond to various species and electromagnetic waves. These desired attributes that *MXene* encompasses have led to many applications [14]. *MXene* applications are presented in table 2. The first explored *MXene* application was seen in energy storage [14]. Moreover, *MXene*s have set ways in the biomedical field and became one of the hottest research topics with studies on photothermal therapy of cancer, biosensors, dialysis, and neural electrodes. Furthermore, due to *MXene*s electromagnetic properties it has been applied in electromagnetic applications, including electromagnetic interference shielding and printable antennas [14]. *MXene* has also been utilized in other fields, including electronic and structural applications like supercapacitors as well as sensing and optoelectronics.

Table 2. Different specific applications of *MXene*s for the generalized field of study.

Field of Study	**Specific applications**
Energy storage and conversion	Sodium-ion batteries, lithium-ion batteries, non-lithium-ion batteries, Li-S batteries, K-ion batteries supercapacitors, lithium-ion capacitors, electrochemical capacitors, hybrid capacitors, hydrogen storage, photocatalyst for direct solar energy utilization, photovoltaic devices, and thermoelectric power generation
Sensors	Mechanical sensors, gas sensors, Solid-state gas adsorptive sensors, Piezoresistive wearable sensors, photoluminescent sensors, terahertz sensors, biosensors, chemical sensors, sensors for macromolecules and cells
Electronics and Photonics	Electrical contacts, conductive fillers, energy harvesting, , piezoelectric materials, thermoelectric materials, and optoelectronics
Catalysis	Electrocatalysis, photocatalysis, CO catalyst, CO_2 reduction O_2 evolution electrocatalyst, H_2 generation, oxygen reduction reaction (ORR), Catalyst for NH_3 synthesis from N_2
Water purification	Membrane separation, toxic heavy metal Cr(vi) adsorption, Lead adsorption, Phosphate sequestration, freestanding membranes for the charge- and size-selective rejection of ions and molecules, dye adsorption, radionuclide pollutant adsorption
Biomedical	Antibacterial, bioimaging, biosensing, therapeutics, and nanomedicine

Chapter 2 - Material and Methods of Synthesizing $Ti_3C_2T_x$ *MXene*

2.1 Chemicals and Materials

In this chapter, the preparation of *MXene* conductive inks via minimally intensive layer delamination (MILD) method and dispense printing using Voltera machine are described. Commercial Titanium aluminum carbide (Ti_3AlC_2) MAX powder was purchased from Nanochemazone, Chemazone Inc., (Canada), 99.6% purity, 400 mesh size, was prepared by high sintering temperature sintering method. $Ti_3C_2T_x$ was formulated by a layer delamination procedure. Etchant to exfoliate Ti_3AlC_2 was developed by Lithium fluoride (LiF) purchased from Aldrich with a -300-mesh size and Hydrochloric acid (HCl) was purchased from Sigma-Aldrich, AR grade, 36.5-38.0 wt%. Distilled water is ultrapure (TYPE 1) water taken retrieved from Millipore Sigma Direct-Q 3 UV system. The pH paper was purchased from Hydrion Micro Essential Laboratory. Vacuum filter paper membrane was purchased from MF-Millipore^{TM} 0.45 µm pore size mixed cellulose membrane 47 mm diameter, hydrophilic, and nonsterile. To gain 0.1M of PBS, Sodium phosphate monobasic dihydrate and Sodium phosphate dibasic dodecahydrate were both purchased from Sigma-Aldrich and both powders were dispersed into 200 mL of distilled water. 4- Nitrophenol (4-NP) was purchased from Sigma-Aldrich and was mixed into 50 mL of distilled water to get 2 mM of 4-nitrophenol. All chemicals and reagents were used as received without further purification.

2.2 MXene Synthesis

Many *MXene* literatures describe the usage of concentrated HF being the etchant of alternative to selectively remove Aluminum from Ti_3AlC_2 [18]. Nevertheless, the implementation of 5 wt% HF is a possible way of bypassing the usage of high HF concentrations. The substitute method undergoes the in-situ formation from hydrogen fluoride such as LiF to prepare etchants

containing 3-5 wt% HF. The MILD method provides many advantages such as simplifying the synthesis method because sonication is replaced with manual shaking, which results in larger and less defective single flakes of *MXene* over getting bulk stacked *MXene* in HF method [18]. The exploration and discovery of the 2014 in situ HF etching method has further enhanced the scalability and production of *MXene*. As shown in figure 2 it displays a general map for $Ti_3C_2T_x$ synthesis formed from Ti_3AlC_2. For the etching procedures reported in this literature, there are two routes one being HF and in situ HF. In the HF route, three different concentrations with different durations were used, which was sufficient to synthesize $Ti_3C_2T_x$. Furthermore, in situ HF route is an alternative way compared to the direct use of hazardous HF, in which the resulting $Ti_3C_2T_x$ multilayered powder behaves like clay in comparison to powders produced by NH_4HF_2 [18]. Delamination of $Ti_3C_2T_x$ powder heavily depends on the chosen synthesis routes. Regarding the HF route or a salt like NH_4HF_2, delamination can be achieved by the introduction of large organic molecules such as dimethyl sulfoxide (DMSO) Toretramethylammonium hydroxide (TMAOH) followed by sonication, if required. In the case of lithium fluoride with hydrochloric acid (LiF/HCl), the resulting Li^+ intercalated $Ti_3C_2T_x$ clay can be delaminated by sonication (clay) or without sonication (MILD) depending on the concentration of LiF and HCl used to prepare the etchant.

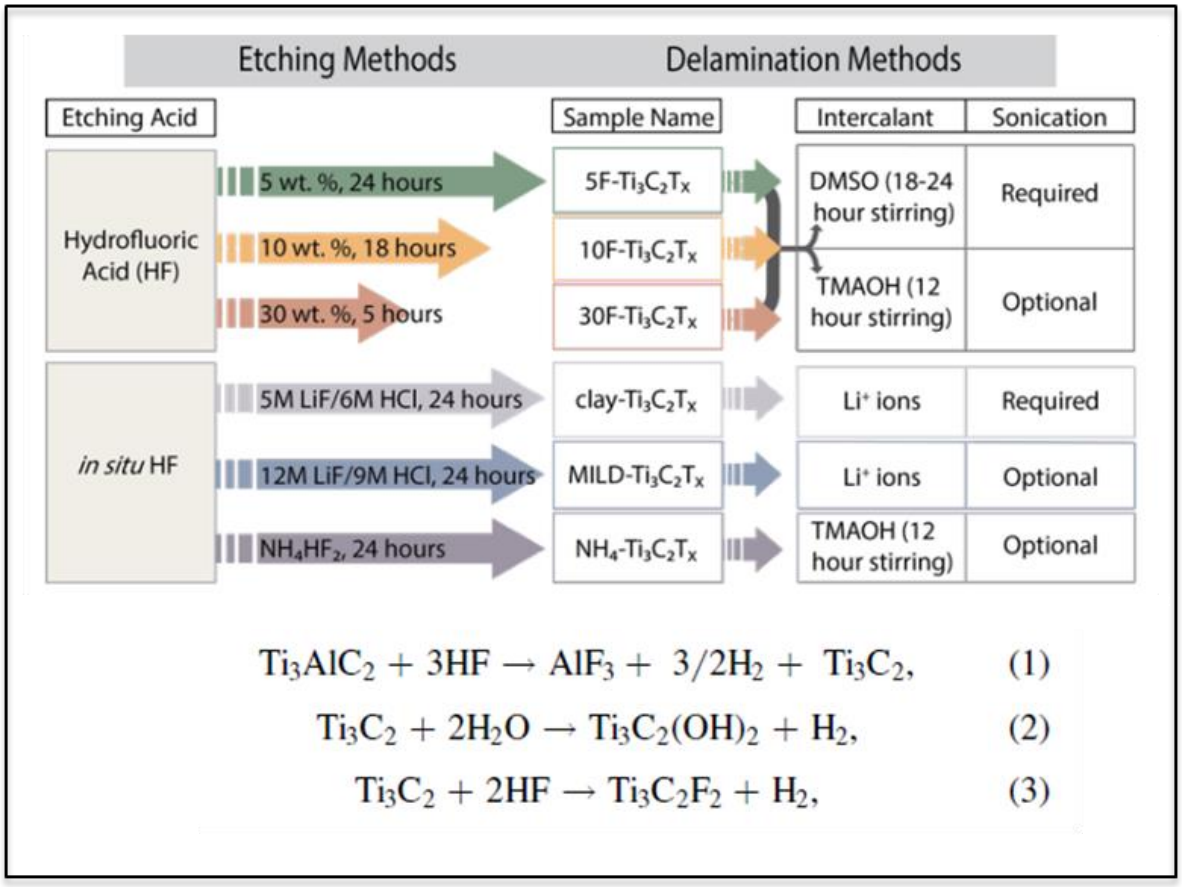

$$Ti_3AlC_2 + 3HF \rightarrow AlF_3 + 3/2H_2 + Ti_3C_2, \quad (1)$$

$$Ti_3C_2 + 2H_2O \rightarrow Ti_3C_2(OH)_2 + H_2, \quad (2)$$

$$Ti_3C_2 + 2HF \rightarrow Ti_3C_2F_2 + H_2, \quad (3)$$

Figure 2: Different synthesis etching routes of $Ti_3C_2T_x$ *MXene,* and equation (1-3) shows actual etching out Al from MAX during exfoliation process. (reproduced by permission from Ref [18])

The preparation of $Ti_3C_2T_x$ was conducted by etching Ti_3AlC_2 using LiF and HCl (12M LiF/9M HCL) at a temperature range from 30 to 45°C as follow: The etchant was prepared by slowly adding 1.6 g of LiF to 20 mL of 9 M of HCl and left under continuous stirring for 10 min for complete dissolving at 45 °C and 200 rpm. Measuring out a total of 1 g of Ti_3AlC_2 powder was then gradually added into the above mixtures where the reaction continued for 48 h with magnetic stirring at 200 rpm for 45 °C to fully remove the interlayer of aluminum. In order to obtain optimum exfoliation conditions, etching experiments were conducted by varying different etching temperatures (27 – 50 °C) and times (24 – 48 h) see table 3.

The acidic solution was washed with deionized water using the Hermle Labortechnik GmbH, model Z 36 HK via centrifuge. The solution was rinsed for 19 washing cycles for 5 min at 3500 rpm and vortex was used in between each washing cycle before the tube was placed back into the machine for the next washing cycle. The centrifugation process was repeated by adding 4 L of deionized water and this process was continued until the pH value of the supernatant reached between 6 to 7. The exfoliation process was conducted by the solution being transferred into one centrifuge tube for one cycle by vortex and then centrifugation at 3500 rpm for 15 minutes. Discarding the supernatant from the final centrifuge process, where unetched MAX and exfoliated few-layers of *MXene* were separated, 60% of the upper part of the *MXene* clay was extracted from the tube and placed into an orange cap tube while adding 40 mL of deionized water, then vortex for 15 minutes. To measure the concentration, 100 µL of *MXene* stock solution was pipetted out and drop cast onto a 0.45 µm MCE membrane filtration paper and placed under an infrared lamp to fully dry. Weight comparisons between wet solution and dried solution were calculated to determine how much unknown stock solution is needed to achieve *MXene* freestanding film. An unknown amount of stock solution is combined with 5 mL of deionized water and vortex for 5 minutes and pipetted out of the tube into a vacuum setup where the process of vacuum filtration occurs to obtain *MXene* freestanding film. Once vacuum filtration is completed, the film is left to dry for 24 h at room temperature. Fully dried freestanding film undergoes resistivity test using Klein Tools Insulation Resistance Tester ET600.

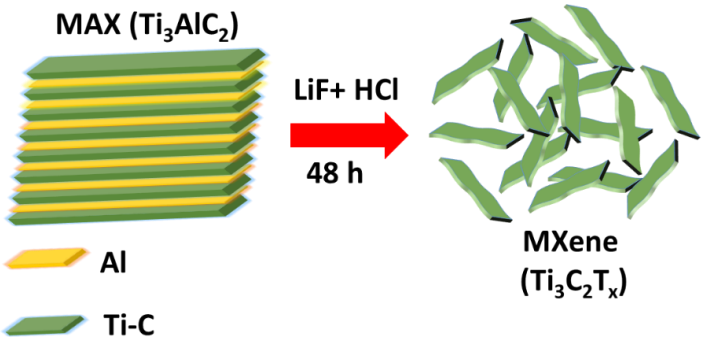

Figure 3. Schematic of *MXene* exfoliation from MAX phase.

Table 3. *MXene* Experimental Conditions.

Sample Code	Reaction Time	Temperature (°C)
MX-1	24	35
MX-2	48	45
MX-4	24	45
MX-5	48	45
MX-7	48	45

2.3 Preparation of MXene Ink

The resulting suspension of MXene clay was placed into a centrifuge tube for one cycle at 15000 rpm for 15 minutes, discarding the supernatant and extracting the clay out of the tube to gain the desired concentrated $Ti_3C_2T_x$ water-based inks. To gain a high concentration of *MXene* solution the solution was centrifuged several times to obtain enough $Ti_3C_2T_x$ sediment. To collect a low concentration of *MXene*, 1 mL of distilled water is added to the sediment each time until the desired concentration is reached and vortex for 5 minutes.

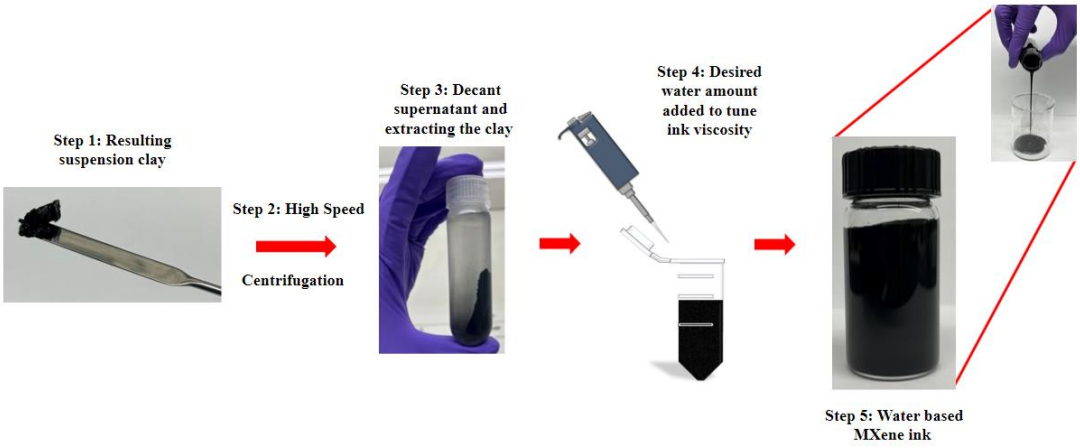

Figure 4: Schematic diagram showing water-based $Ti_3C_2T_x$ *MXene* inks preparation.

2.4 Printing

Printing is an additive manufacturing technique that offers many possibilities for simple, large-scale, and low-cost device fabrication. In contrast, to conventional silicon-based electronics or gas-phase deposition techniques, which require sophisticated and lengthy manufacturing processes, printing is done in a maximum of three steps: pretreatment of the substrate, printing, and post-treatment. Despite the many great advancements in printing technologies, functional printing, and ink development are still being explored. This is mainly due to the difficulty of developing additive-free, high-performance inks [29]. *MXene*s can change the printing world by offering exceptional possibilities to produce such inks as discussed before. *MXene*s are still in the early stages of development; their printing is currently limited to the technique used in research labs [29]. So far, only three printing methods including screen-printing, inkjet, and extrusion printing have been reported for processing *MXene*s [29].

2.4.1 Screen Printing

Screen-printing (SP) is a fast and efficient contact printing method where ink is deposited on a substrate through a mesh with an open printing pattern and non-printing areas. Compared to other printing methods SP is very simple and inexpensive. This method is mainly utilized for the deposition of thick films that range from 1–100 μm. The SP has the capabilities to be done in automated mode where sheet-to-roll occurs and exhibits printing speeds that can reach up to 70 m/s [29]. It provides easy fabrication due to the screens making this process a very fast prototyping method. The fabrication of screens is simple and requires little training and tools, which makes it widely accessible [29]. However, despite the signs of progress within this method, formulation of screen printable *MXene* inks requires further attention since aqueous inks suffer from fast evaporation of the solvent (water) causing an increase in the viscosity of the inks and shortens the printing time which is not suitable for industrial applications [29]. Unfortunately, organic solvents such as DMSO are capable of dispersing high concentrations of *MXene*'s but are not compatible with the conventional emulsions, which are used for making screen-printing screens making it important that developing organic inks in less aggressive solvents is strongly required.

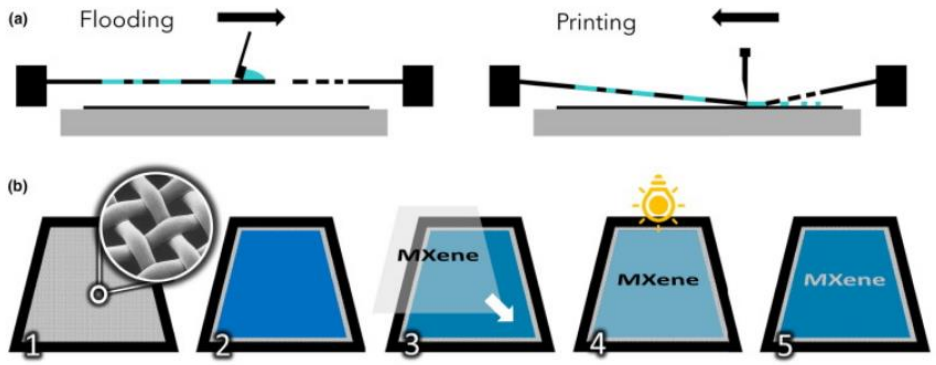

Figure 5: Screen-printing of *MXene*s inks. (reproduced by permission from Ref [29])

2.4.2 Inkjet Printing

Inkjet printing (IJP) is a digital non-contact method, which is vastly used in both research and industry. IJP is one of the best techniques for parameter optimization, and fast prototyping since the printing pattern is provided to the printer as a digital file (can be modified easily) and ink consumption is very low (1-2 mL) [30]. Based on the droplet generation mechanism, there are two main types of inkjet printing, continuous inkjet printing (C-IJP) and drop-on-demand inkjet printing (DOD-IJP). The inkjet printing method allows printing paths with a high resolution and line width down to 50∼80 μm and is thus extremely suitable for printing prototype devices on the lab scale [30]. However, its working mechanism implies a low printing throughput, which leads to limitations in its application of scalable printed electronics.

2.4.3 Extrusion Printing

Extrusion printing is a gel-like ink (solid-like behavior) is extruded as a filament through a nozzle and deposited on a desired substrate. Extrusion printing has been used for both two-dimensional and three-dimensional printing of materials. However, to print three-dimensional it requires more specific rheological properties to be able to print in a layer-by-layer manner [29]. Whereas two 2D extrusion printing is suitable for the deposition of thick films and structures with very high conductivities. It has been reported that extrusion-printed structures are robust and show great flexibility [29]. Extrusion printing is a versatile method that can also be used for the fabrication of freestanding devices.

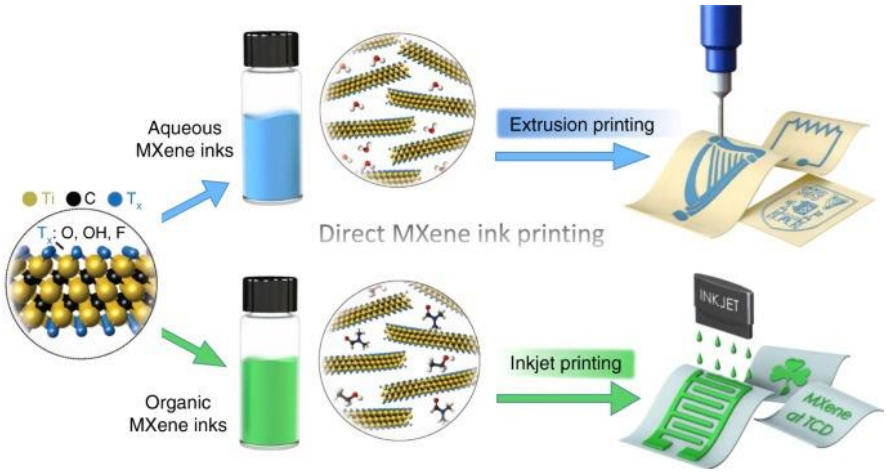

Figure 6: Extrusion and Inkjet printing of *MXene.* (reproduced by permission from Ref [29])

2.5 Electrochemistry

Electrochemistry is a powerful tool to probe reactions involving electron transfers [31]. Electrochemistry relates the flow of electrons to chemical changes caused by the pathway of electric current and the production of electrical energy by chemical reactions. In inorganic chemistry, the resulting chemical change is often the oxidation or reduction of a metal complex. For instance, in electrochemistry, there can be a chemical reduction and an electrochemical reduction that occurs. In chemical reduction, it is able to occur due to electron transfers from a chemical solution where the lowest unoccupied molecular orbital is at a lower energy than the electron in the highest occupied molecular orbital of a solution. The transfer of an electron between the two molecules in solution is thermodynamically favorable and the difference in energy levels is the driving force for reactions [31]. Therefore, in an electrochemical reduction, solutions can be reduced via heterogeneous electron transfer from an electrode. This occurs due to the presence of an electrode as an electrical conductor [31]. In electrochemistry, most electrodes are typically platinum, gold, mercury, or glassy carbon. Furthermore, through the use of an external power source like a potentiostat, the voltage can be applied to the electrode to help modulate the energy of electrons in the electrode [31]. Once this action takes place, the electrons in the electrode are at

a higher energy causing an electron from the electrode to be at a lower concentration due to the energy difference between that of the electrode and the solution. In order to change the driving force of a chemical reduction, changing the identity of the molecule used as the reductant is needed. The power of electrochemistry resides in the simplicity with which the driving force of a reaction can be controlled and the ease with which thermodynamic and kinetic parameters can be measured [31].

2.5.1 Cyclic Voltammetry

Cyclic voltammetry (CV) is a powerful and popular electrochemical technique commonly employed to investigate the reduction and oxidation processes of molecular species [31]. The traces showcased in Figure 7 are called voltammograms or cyclic voltammograms (CV). The *x*-axis represents the parameter applied potential (*E*), while the *y*-axis is current (*i*) which represents the response.

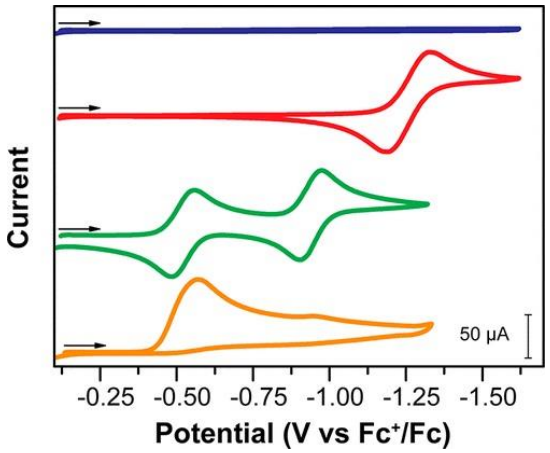

Figure 7: Cyclic voltammograms profile. (reproduced by permission from Ref [31])

Two conventions are commonly used to report CV data, one being the US convention and the other being the IUPAC convention. Furthermore, seldom is a statement provided that describes the sign convention used for acquiring and plotting data [31]. CV traces contain an arrow, which indicates and symbolizes the direction in which the potential was scanned to help record data. For

instance, the arrow indicates the beginning and sweep direction of the first segment also known as a "forward scan". A very important parameter in cyclic voltammetry data is the scan rate (υ). It indicates that during the experiment the potential was varied linearly at the speed (scan rate) in the units of mV per second. Overall, the scan rate controls how fast the applied potential is scanned. Faster scan rates lead to a decrease in the size of the diffusion layer; consequently, higher currents are observed [31].

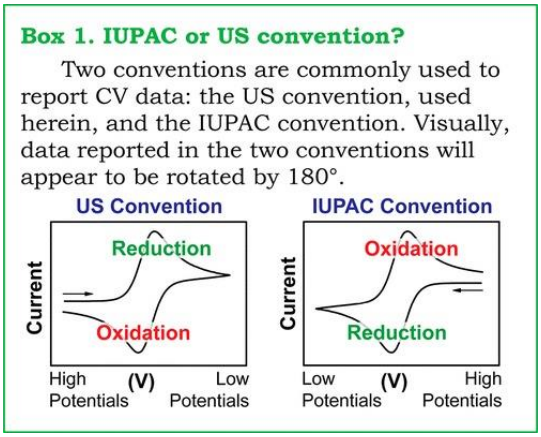

Figure 8: Two conventions that are used to report CV data. (reproduced by permission from Ref [31])

The presence of peaks in a CV occurs due to the equilibrium between solutions by the Nernst equation $E = E^0 + \frac{RT}{nF}\ln\frac{Ox}{Red} -= E^0 + 2.3026\frac{RT}{nF}\log_{10}\frac{(Ox)}{(Red)}$. The Nernst equation relates the potential of an electrochemical cell (E) to the standard potential of a species (E^0) and the relative activities of the oxidized (Ox) and reduced (Red) analyte in a system at equilibrium. In the equation, F is Faraday's constant, R is the universal gas constant, n is the number of electrons, and T is the temperature. The Nernst equation provides a powerful way to predict how a system will respond to a change of concentration of species in solution or a change in the electrode potential [31].

Chapter 3 - Instrumental Characterization

The goal of the present chapter is to describe the instruments used to characterize *MXene* material, dispense printing technology that was used to fabricate printed sensors, and electrochemical performance tests of the optimized *MXene* ink printed sensors were studied. The structure and morphology of the prepared *MXene* materials were characterized using scanning electron microscopy (SEM), X-ray powder diffraction (XRD), atomic force microscopy (AFM), transmission electron microscopy (TEM), X-ray photoelectron spectroscopy (XPS), Raman spectroscopy, and four-probe electrical measurements were employed to characterize *MXene* material.

3.1 X-ray Powder Diffraction (XRD)

X-rays are a form of electromagnetic radiation capable of penetrating solid materials up to several nanometers from their surface to probe the crystal structure of any given crystalline or amorphous solids, glassy solids, and even polymers [33]. They are also indispensable to measure molecular crystals such as proteins, and various powders of microcrystalline and nanocrystalline in nature. As such, there are different versions of X-ray diffraction (XRD) machines, commonly called XRD diffractometers. The discussion in this chapter is solely related to crystalline solids. Later in Chapter 4, the results are obtained from the bulk crystal structure of MAX phase material and nanoscale crystal structures of *MXene* derived from the MAX phase crystals. The beam in an XRD diffractometer typically is diffracted from the periodic crystal atoms and gets constructive interference to produce high-intensity peaks, as shown in Figure 9 below.

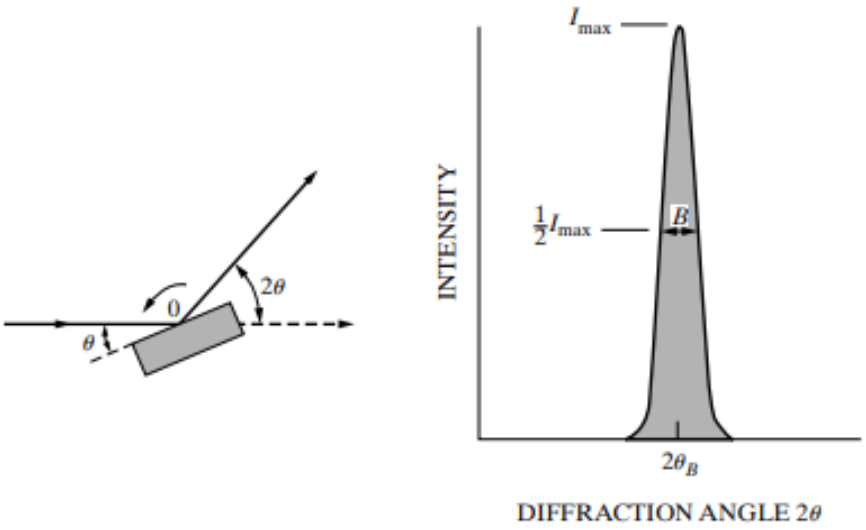

Figure 9. Schematic of X-ray diffraction from a crystal, where the high-intensity peak is obtained at an angle θ, called Bragg angle θ_B [33].

Bragg's law:

$$2dsin\theta = n\lambda$$

The primary diffraction law is generally satisfied at this angle and the corresponding intensity pattern is obtained in the X-ray diffraction pattern. In this equation, *d* is the interplanar spacing in the crystal between the crystal planes of a given crystal lattice. It is connected to the planar indices of the crystal, which in turn is related to the crystal structure parameters. A more complicated crystal structure is relatively difficult to solve the equation, the simplest one being a cubic crystal. Letter *n* stands for the order of diffraction, which is often taken as 1, and λ stands for the wavelength of the X-ray. For a general powder diffraction diffractometer, a Cu Kα radiation source is used with an x-ray wavelength value of 1.5406 A^0, with corresponding x-ray energy of 8.04 keV.

3.2 Scanning Electron Microscope (SEM)

Scanning electron microscopy (SEM) is one of the many-electron microscopy techniques that is routinely used for analyzing various physical (including morphological features), chemical, compositional, and phase (crystallographic phase) information. In addition, the SEM tool has been increasingly coupled with other experimental tools (such as electron beam-related lithographic use) to bring technological advances. It is also being used to characterize a wide variety of samples, from electronic materials to polymers, biomaterials, and biological materials [34]. To characterize the samples in ambient and special environments, environmental SEMs are also in high demand. Other detectors are being used with an SEM to extract more information, a few such detectors are secondary electron (SE) detectors, backscattered electron (BSE) detectors, and energy dispersive x-ray analysis (EDX) detectors.

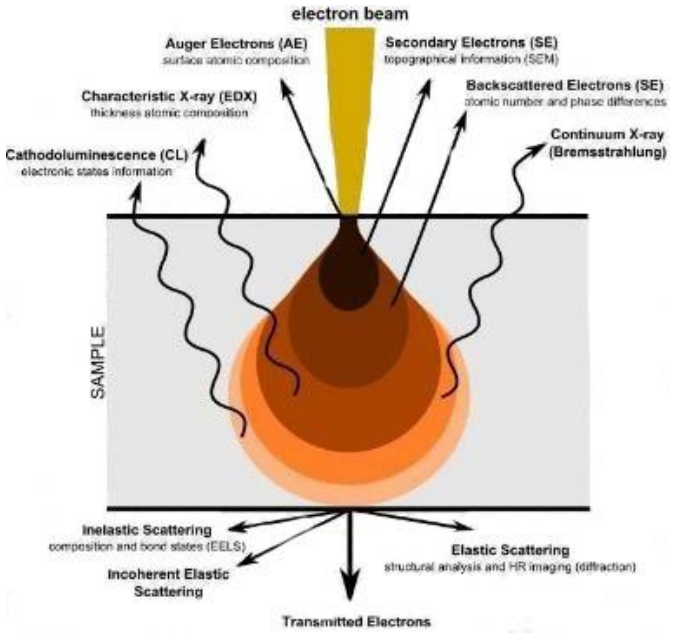

Figure 10. Different types of signal generation at the sample surface because of electron-matter interaction [34].

Figure 10 above shows the interaction volume and the associated electronic and photonic signal generation at the sample surface due to the incident electron beam (vertical yellow column at the top from SEM electron source) and matter (sample surface and volume near the surface) interaction. Detecting each of the signals provides a unique physics and chemistry of the sample in addition to the physical structure. In typical SEMs, detectors for SE, BSE, and EDX are commonly installed for analyzing the electrons and photons for material analysis.

3.3 Atomic Force Microscopy (AFM)

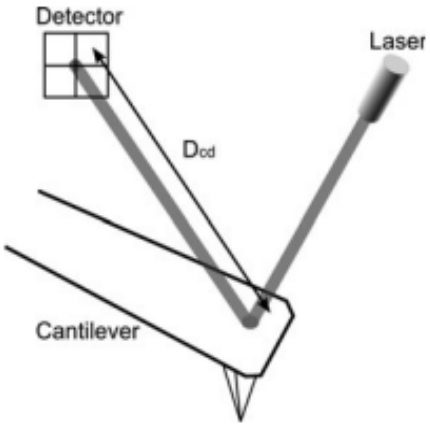

Figure 11. Schematic picture of an AFM head, showing a fine laser source, the cantilever, and a detector to collect the deflected light [35].

Atomic force microscopy (AFM) is a novel technique that is routinely used to see and measure the surface structure with very high resolution, in principle, to the atom scale. The technique generally falls under a collection of similar experimental principles, called scanning probe microscopy (SPM). For example, for atomic resolution images, scanning tunneling microscopy (STM) is used where one can make atom scale analysis (required ultra-high vacuum and cryogenic temperature conditions to freeze the atomic positions and avoid surrounding air particles). Nevertheless, a reasonably well-maintained AFM can measure ultra-thin (sub-nanometer level) atomically thin and flat surfaces with unprecedented control provided the sample

is clean enough. After its discovery, the technique now can be applied to a wide variety of samples in many different environments, including biological samples in buffer solutions [35]. In addition, the technique has been merged with other analytical techniques, such as electrochemical techniques, to fundamentally open new avenues of scientific discoveries.

In its simplest explanation, the AFM head in a microscope stage consists of three critical elements, a laser source that sends light toward the probe that probes the sample surface, a cantilever with a sharp cantilever tip that acts as the probe, and a detector that detects the laser beam after it gets deflected from the probe head (cantilever tip). Typically, a detector consists of a quadrant photodetector system that processes the signal in a certain way that minimizes the noise and maximizes the signal using electronics and feedback control. Apart from the above three components, the control electronics with feedback control and a computer using specially designed software are also very important parts of this instrument.

3.4 Transmission Electron Microscopy (TEM)

Transmission electron microscopy (TEM) imaging is an electron microscopy technique like SEM. However, unlike SEM, which studies surface properties of the sample such as surface micrograph, a TEM looks at the internal structure of the specimen, including the crystal structure of the sample. In a TEM electron beam penetrates through the specimen thereby interacting with the internal structure of the sample and carries the internal structure information, including the atomic arrangements of the atoms present in the sample. Typically, the sample thickness must be very thin (maximum thickness ~ 50 nanometers) to penetrate into the structure, making it ideal for atomically thin two-dimensional materials (2D materials) and other nanoscale materials. For bulk crystals, a more rigorous sample preparation method is needed where another piece of equipment called a focused ion beam (FIB) is used to prepare a slice of the specimen (~ 50 nanometers or

thinner) from the bulk sample for TEM imaging [36]. The following schematic diagram shows the internal arrangement of various parts of a TEM machine.

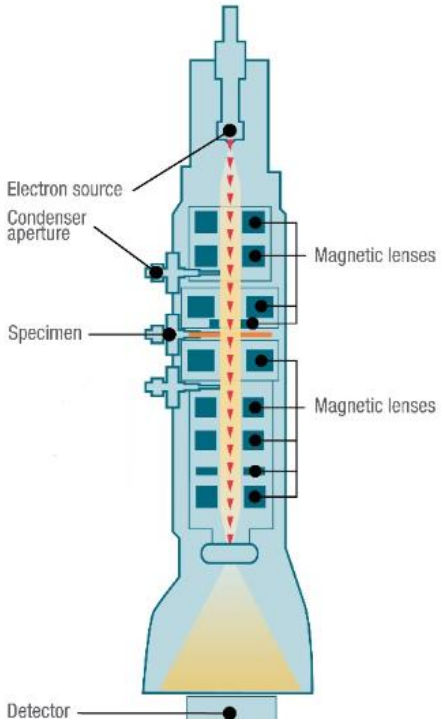

Figure 12. Schematic presentation of a TEM tool, showing its internal structure [36].

As shown in above picture, the TEM has three broad sections inside the microscope system: (1) The illumination system, (2) The objective lens and specimen stage, and (3) The imaging system. The electron source, electron accelerator, condenser lens and condenser aperture constitute the illumination system. Several magnetic stages and electron beam optics (such as stigmation) consist of the objective lens and specimen stage. A few more imaging lenses and CCD camera constitute the imaging system. Finally, specialized electronics and electronics systems and various cooling arrangements of high voltage electronics involved in the instrument are indispensable components of the TEM instrument. In a modern TEM system, several accessory measurement attachments are often found such as EDX (energy dispersive X-ray analysis) and EELS (electron energy loss spectroscopy).

3.5 X-ray Photoelectron Spectroscopy (XPS)

X-ray photoelectron spectroscopy (XPS), originally known as electron spectroscopy for chemical analysis (ESCA), is one of the most informative analytical tools used for surface analysis of a wide variety of materials. As the name suggests, it derives qualitative and quantitative information about the chemical and environment (such as the chemical bonding environment) analysis from the sample surface (typically, from a few nanometers depth from the surface). From the macroscopic sample, a surface as high as sub-10 micrometer spatial resolution can be obtained for this spectroscopic measurement using a dedicated XPS instrument [37]. The technique is widely used not only in academic and industrial research but is also a valuable tool for various technological industries that are related to the chemical industry, nanomaterial industry, thin-film industry, and solar industry to name a few.

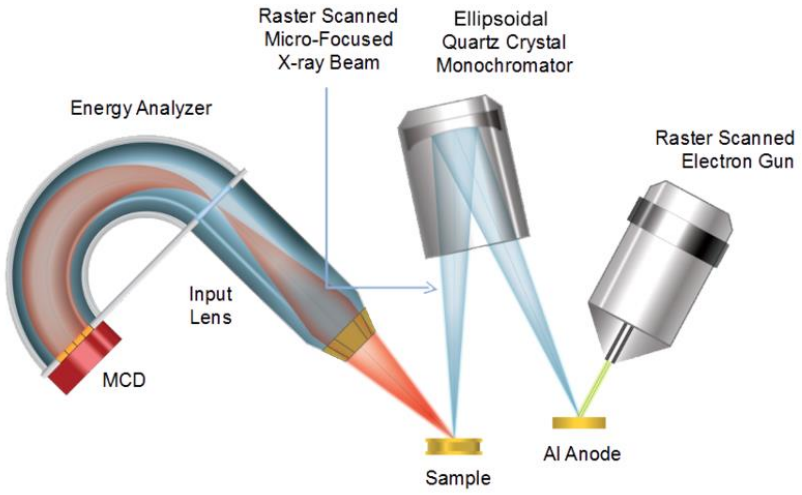

Figure 13. Operational principles of an XPS tool [37].

The operational principle of an XPS instrument is based on the energy and energy distribution of X-ray photoelectrons obtained from the sample surface. As shown in Figure 13, electrons from a gun hit an aluminum anode exciting the aluminum atoms and subsequently producing Al Kα x-rays. These X-rays undergo a monochromator and get raster scanned and

micro-focused onto the sample surface. Photoelectrons are generated during this process that are guided towards an electron energy analyzer. The analyzer, due to its hemispherical architecture, resolves the energy of the photoelectrons on an MCD detector. From this spectral resolution, the binding energy (energy of the photoelectrons) and the intensity (number of photoelectrons at a given binding energy) are extracted. This information for elemental materials has been documented and serves as a reference for the identification of elemental identity and chemical state of an unknown material. When analyzing specific material using XPS, therefore, unique characteristics of the chemical bonding environment are sought.

3.6 Raman Spectroscopy

Raman spectroscopy is an invaluable spectroscopic characterization method that is used for studying the vibrational energy spectrum of the material when excited with an external source such as a laser beam and measuring the frequencies of the scattered light. Thus, the method serves as a fundamental technique to identify the bonding environment of any given solid and the vast majority of materials, including biomaterials and biological materials [39]. The method is widely popular among many industries such as semiconductors, chemical, pharmaceuticals, and biomedical industries. Over the years, the technique has been transformed into more sophisticated ones such as surface-enhanced Raman spectroscopy (SERS) and tip-enhanced Raman spectroscopy (TERs) [39].

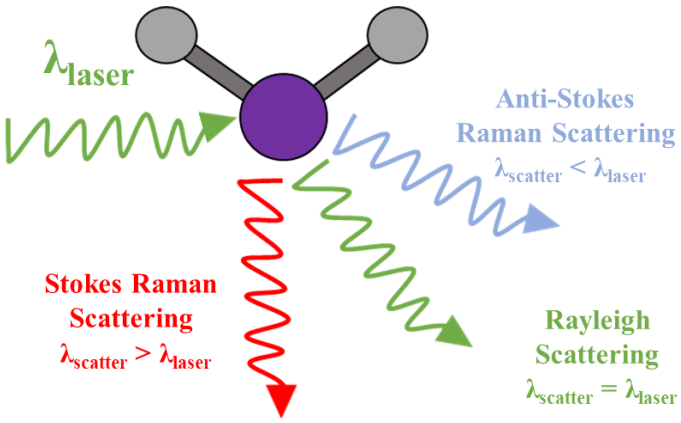

Figure 14. The operational principle of Raman spectrum of a molecule.

Figure 14 above depicts the comparison of the energy of the incident light with the energy of the scattered light for a molecule (the same basic principle holds with any solid). Furthermore, the scattered light has three different energies – energy with similar frequency to the incident light (called Rayleigh scattering, an inelastic scattering). Energy with a lower frequency to the incident light (called Stokes scattering, and inelastic scattering), and energy with a higher frequency to the incident light (called Anti-Stokes scattering, and inelastic scattering). Depending on the molecular and/or solid structure in each crystal, the Stokes and/or Anti-Stokes scattering serves as the signature of the crystal symmetry and crystal structure. In a more realistic way, Raman spectroscopy is also used to study several other information such as defects in crystals, various functional groups attached to the crystal, stress-strain study, degradation study, etc., making Raman one of the invaluable measurement techniques for solids.

3.7 Four-Probe Electrical Conductivity

Electrical properties are one of the fundamental properties of the materials that help categorize materials as insulators, semiconductors, and metals, although there are other forms of electrical properties such as superconductors and semimetals [40]. It is one of the fundamental areas of physics and continues to advance our knowledge to the frontiers of science. However, the

measurement techniques yet unravel the intricacies of practical devices, and adequate efforts are needed to overcome the bottlenecks in understanding the true electrical conductivity of the material. Four-probe electrical conductivity (or four-probe electrical resistivity) measures the true electrical conductivity (or electrical resistivity) of a sample of thin film or printable form by eliminating the contact-related issues such as contact resistances that often arise from metal-semiconductor junctions.

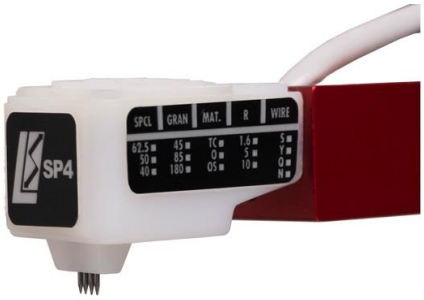

Figure 15. Electrical probe-head of a four-probe electrical conductivity measurement system [40].

The picture shows (Figure 15) a commercial probe head of a four-probe electrical conductivity measurement system from Signatone, where an electrical current (I) is applied to the sample surface through two outer probes and the change in the voltage (ΔV) is measured between the two inner probes when the four probes touch the sample (specimen) surface, and a measurement is conducted. Based on this, sheet resistance and sheet resistivity are calculated as follows: [40]

$$R_s = \left(\frac{\pi}{\ln 2}\right)\left(\frac{\Delta V}{I}\right) = 4.53236\frac{\Delta V}{I}$$

$$r = R_s . t$$

Where t is the thickness of the sample.

3.8 Dispense Printing via Voltera V-One

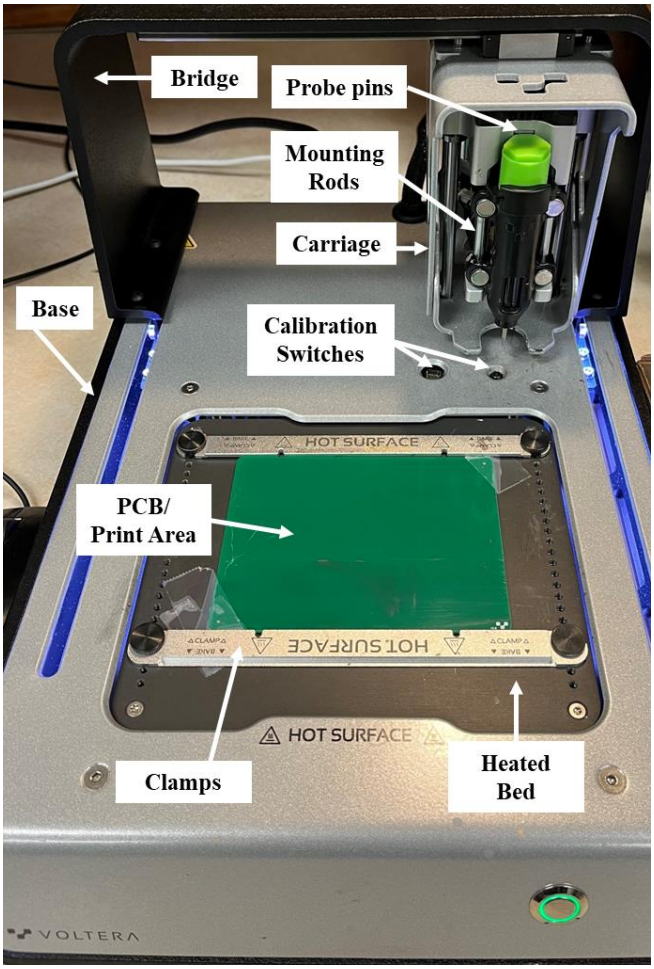

Figure 16: Voltera V-One dispense printing technology.

The *MXene* conductive ink sensor fabrication process was done via dispense printing by a PCB circuit design system (Voltera V-One, Canada). Printing parameters were optimized for *MXene* inks on various flexible substrates (Thick polyimide sheet, KOH-treated polyimide sheet, non-KOH treated polyimide sheet, photo sheet, and thick photo sheet). KOH substrate treatment solution was prepared by 1 M of KOH in 1000mL of distilled water. Cleaned polyimide substrates were washed in prepared KOH solution for 30 mins in bath sonication. Afterwards, the KOH-treated substrates were rinsed with distilled water and isopropanol. Lastly, a nitrogen gun to dry the substrates and then safely store the treated polyimide substrates in a vacuum chamber. To

dispense quality features a nozzle with an internal diameter of 100 μm was used. The sensor electrodes have a feature size of a working area of 3 mm and a contact area of 7 mm by 2 mm. The rheological ink properties (viscosity) of *MXene* ink are important when printing with Voltera-V One technology. Utilizing the right ink concentration helps minimize the occurrence of having a clogged nozzle. 1mg/mL and 0.5mg/mL of *MXene* ink concertation were both used during the fabrication process of printing *MXene* sensors.

The influence and proof of quality of all the printing parameters onto the substrates were experimentally observed through soluble adhesion test. After printing, each substrate was placed into 40 mL of deionized water for 72 hours (Figure 17). Electrical property characterization of printed electrodes was performed using a digital multimeter where resistance was measured before and after being submerged in distilled water (Tables 4-5). It is seen in Table 5 after printed electrodes were placed in the water aqueous solution for three days that the resistance of the electrodes decreased measurements went from ohms to kilo ohms. Based on tables 4-5 from the measured resistance the desired substrates used to further carry printed electrode experiments were non-KOH treat polyimide sheets due to having the best adhesion with *MXene* ink to substrate as well.

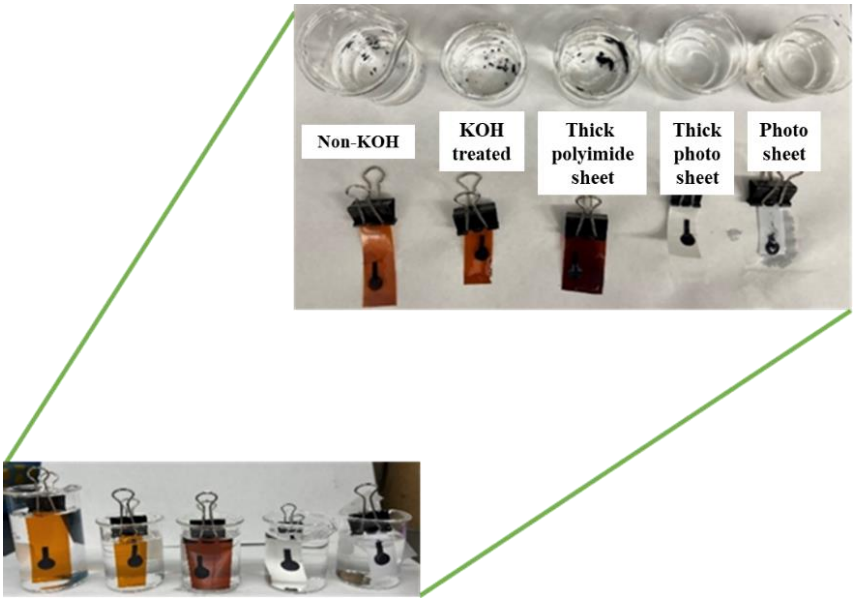

Figure 17: Electrodes submerged in distilled water for 72 h.

Table 4. Voltera printed *MXene* electrodes resistivity before submerged into distilled water for 72 h.

Sensor	Substrates				
	Thick Sheet	**Non-KOH polyimide**	**KOH treated polyimide**	**Thick Photosheet**	**Photosheet**
1	9.2 Ω	18 Ω	9.9 Ω	7.4 Ω	13.3 Ω
2	7.0 Ω	11.7 Ω	19.4 Ω	8.1 Ω	28.2 Ω
3	6.0 Ω	12.3 Ω	9.4 Ω	12.3 Ω	32.4 Ω
4	7.7 Ω	14.7 Ω	11.2 Ω	7.5 Ω	21.8 Ω
5	8.8 Ω	22.3 Ω	12.4 Ω	7.8 Ω	24.9 Ω
n/a- more than 5 MOhm					

Table 5. Voltera printed *MXene* electrodes resistance after submerged into distilled water for 72 h.

Sensor	Substrates				
	Thick Sheet	**Non-KOH polyimide**	**KOH treated polyimide**	**Thick Photosheet**	**Photosheet**
1	7.2 Ω	88.6 Ω	74.4 Ω	n/a	n/a
2	8.4 Ω	88.1 Ω	12 Ω	n/a	n/a
3	21.1 Ω	122.9 Ω	n/a	n/a	n/a
4	10.8 Ω	94 Ω	n/a	n/a	n/a
5	n/a	103.1 Ω	13.6 Ω	n/a	n/a

n/a- more than 5 MOhm

3.9 Electrochemical characterization and sensing

The electrochemical measurements were carried out on Gamry Instruments potentiostat (Interface 1010E) from *Gamry Instruments*. Each experiment was conducted at room temperature and performed on a three-electrode setup as shown in Figure 18a where Ag/AgCl (3M NaCl) acting as the reference electrode, counter electrode being a platinum wire, and *MXene* printed electrodes as the working electrode produced from the dispense printer Voltera-V One mentioned in Figure 16. The electrochemical tests were also conducted on bare Glassy Carbon Electrode (GCE) and *MXene*-coated GCE in a standard electrochemical cell system as exhibited in Figure 18b with 0.1 M PBS used as the electrolyte solution and 150 µL of HCL to create a PH of 5 within the electrolyte solution. Techniques like cyclic voltammetry (CV) and differential pulse voltammetry (DPV) were conducted and studied to see the quantitative analysis of different 4-Nitrophenol (4-NP) concentrations. The DPV provides better sensitivity where a sensitive signal curve will be present during measurements. *MXene*/GCE electrodes were prepared by taking a small amount of *MXene* powder into 9 mL of distilled water to gain diluted *MXene* solution and then subjecting to a 15-minute bath sonication. Moreover, 6 µL of the *MXene* solution was dropped onto the pre-cleaned GCE, and then dried under an IR-lamp.

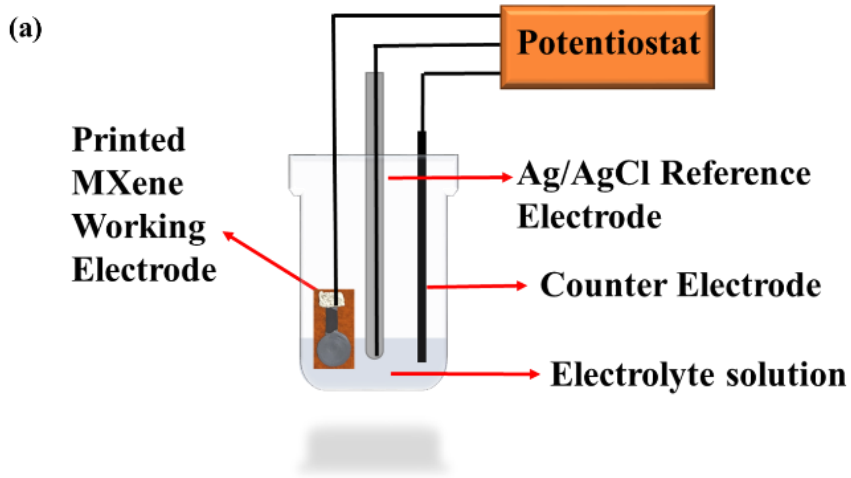

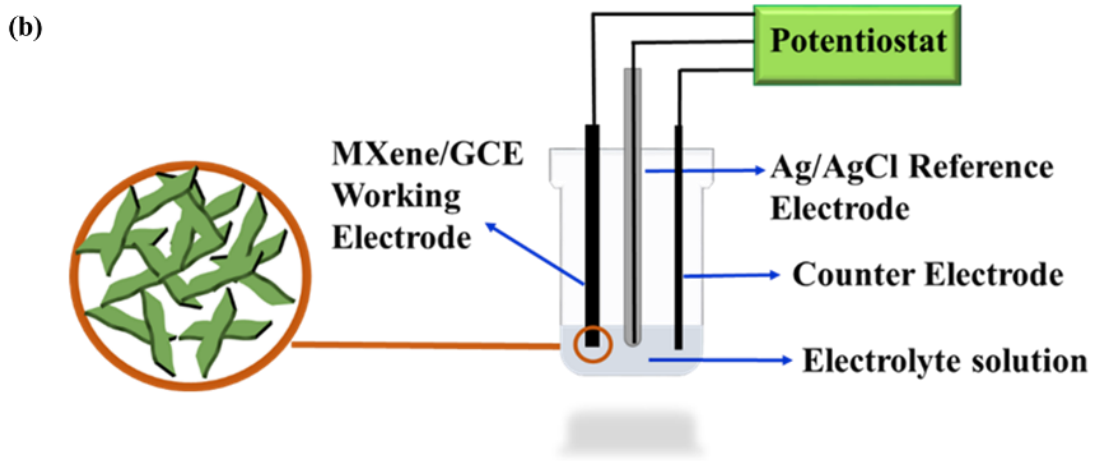

Figure 18. (a) Three-electrode system with printed *MXene* as working electrode in 0.1 M of PBS and HCL solution. (b) Three-electrode system with 6 µL dropped cast *MXene* onto glassy carbon electrode in 0.1 M of PBS and HCL solution pH 5.

3.9.1 Cyclic Voltammetry (CV)

Cyclic voltammetry (CV) is a fundamental electrochemical technique often used to study the redox characteristics of the chemical species in an electrochemical cell. Each of the oxidation and reduction events, associated with electron transfer between the electrode and electrolyte, therefore, brings a peak in the current vs. voltage sweep across the working and counter electrode with respect to the reference electrode. Some of the important information about the electrochemical system obtained from CV are redox behavior, electrochemical kinetics, diffusion vs. adsorption characteristics of charge carriers, concentration analysis, electrode surface properties, and stability and reactivity of electroactive species. The CV measurements was performed for 4-Nitrophenol sensing on bare GCE and *MXene* coated GCE electrode using 0.1 M of Phosphate-buffered saline (PBS) mixed with 150 µL of hydrochloric acid (HCl) to formulate an acidic analyte (PH 5), and different concentrations of 4-Nitrophenol ranging from 100µM - 1000µM.

Chapter 4 - Results and Discussion

4.1 MXene Ink

Synthesis of *MXene* is a top-down method and the flake size produced in the MILD method is directly related to the grain size, and the crystalline quality of the starting MAX powder. The processed $Ti_3C_2T_x$ material can be reprocessed by delamination, size selection, or sonication. Post processing from MAX phase, *MXene* can be shaped in a variety of forms based on its applications, including its deposition as a free-standing film or thin films, painting, or stamping depending on the application as shown in Figure 19. From synthesized *MXene*, highly concentrated $Ti_3C_2T_x$ ink was collected and used for painting and stamping applications. Since the synthesized water based *MXene* ink provides the capability of tuning the viscosity of the ink, it can be used by several printers for various printed *MXene* applications and simply can be used for drop casting and coatings. By diluting the highly concentrated ink, printing was employed and provided printing of *MXene* for precise control over the patten, increasing the amount of ink by increasing the number of layers. Using vacuum filtration, diluted ink also provides conductive *MXene* free-standing film or thin films to be produced.

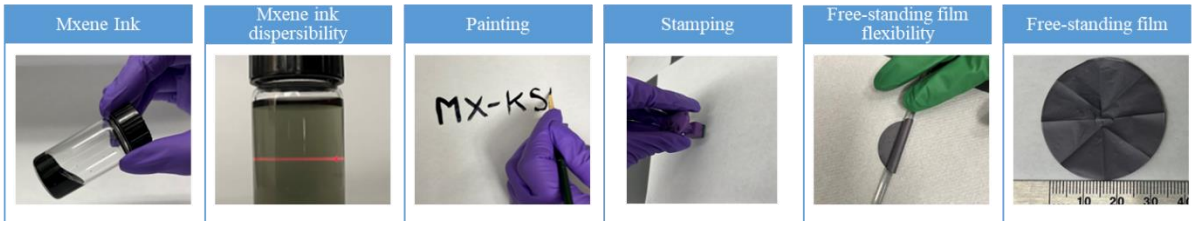

Figure 19. Synthesized $Ti_3C_2T_x$ ink for tunable viscosity, ink dispersibility, painting, stamping, flexible *MXene* free-standing film, and conductive *MXene* free-standing film.

4.1.2 Solvent Exchange

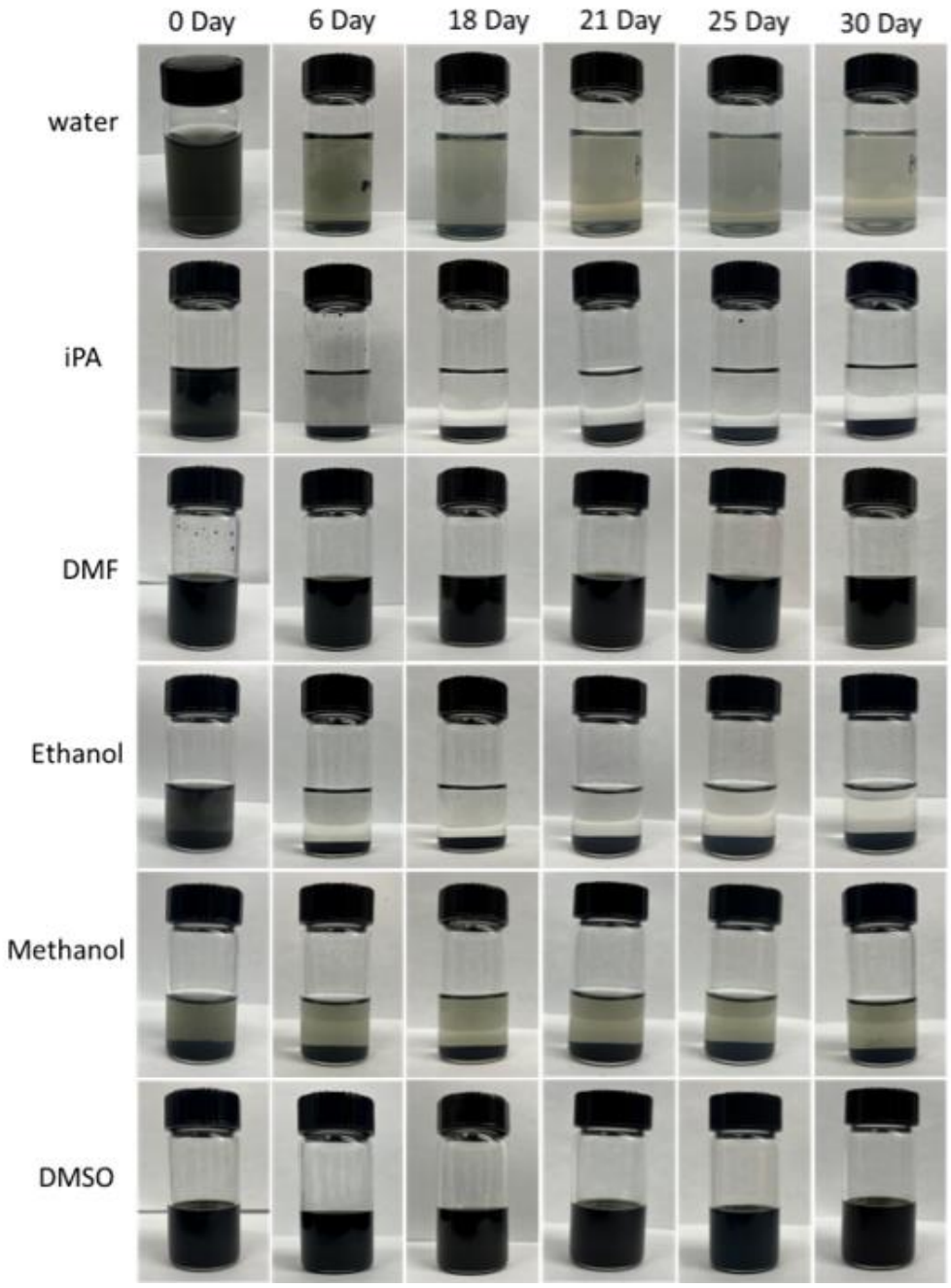

Figure 20. Oxidation stability study of *MXene* ink with several solvents over a 30-day period of testing after formulation of *MXene* colloidal suspension.

The dispersion and oxidation stability of produced *MXene* inks mixed in different solvents were studied. Preparation of *MXene* dispersions was achieved through multiple solvent exchanges

and was conducted 3 times without sonication. To minimize accelerated oxidation of *MXene*s and degradation of their shelf life, *MXene* aqueous mixtures were stored in a low temperature cabinet. As shown in Figure 20, six solvents were used: water, isopropanol (iPA), dimethylformamide (DMF), ethanol, methanol, and dimethyl sulfoxide (DMSO) each were dispersed in *MXene* ink over a period of 30 days. The effect of *MXene*s dispersed in suspensions displayed that dispersing *MXene* nanosheets in DMF and DMSO had the best suspension compared to isopropanol, ethanol, and methanol based on the observation of sedimentation of *MXene* and its deposition at the bottom of the glass vials. Furthermore, the results of *MXene* nanosheets sediments settling at the bottom of the glass vials for ethanol, isopropanol, and methanol compared to DMF and DMSO, which shows that DMF and DMSO are to be the preferred solvents to get a good dispersion of *MXene*. Interestingly, DMF solvent exchange preferably increases the oxidation stability of MXene compared to the water, since water and dissolved oxygen play a major impact in the oxidation of *MXene*s. Therefore, dispersing *MXene* nanosheets in non-aqueous polar solvents can limit the interactions with water and other dissolved oxygen [28].

4.2 X-ray Powder Diffraction (XRD)

X-Ray diffraction measurements is a characterization technique where crystalline features of MAX phase and corresponding *MXene* material can be analyzed, before and after chemical etching, respectively. This measurement technique is the most important characterization method for *MXene* because it indicates if successful exfoliation of *MXene* layers were achieved by the disappearance of the MAX phase peak (104) plane that is related to the element aluminum along with the introduction of new peak. Another indication of successfully exfoliated *MXene* material is by the lower angle shifting in the (002) peak plane. Given the crystal geometry, from the XRD spectra the interlayer *d*-spacing and lattice parameters can be calculated. The lattice parameters

and structural phase of the prepared free-standing film, MAX powder, and *MXene* material were studied using X-ray diffractometer (XRD, PANalytical Empyrean multi-purpose x-ray diffractometer) with Cu-Kα radiation (λ = 1.541Å). The XRD patterns of the starting MAX phase material and resulting *MXene* material are shown in Figure 21 (a-f) for optimizing suitable exfoliation condition. The XRD pattern of the obtained *MXene* material by etching with by MILD route for optimized samples is shown in Figure 22. The identified peaks at 2θ ~ 9.4°, 19°, 33.9°, 36.6°, 38.8°, 41.6°, 56.3°, and 60° correspond to (002), (004), (100), (102), (104), (105), (109), (110) planes of Ti_3AlC_2, respectively [18]. In the figure, the disappearance of high intensity peak position at 38.8° which belongs to Ti_3AlC_2 indicates that *MXene* was completely exfoliated out of the MAX during the etching. The dominant peak for 002 plane shifts to a low angle, which indicates to newly formed Ti_3C_2 *MXene*. Figure 21(b) indicates the chemical exfoliation and conversion of MAX into *MXene* after 48 h etching. Increased etching time showed results of efficient elimination aluminum from the MAX phase compared to etching for 24 h based on Figure 21(a). The lower angle shifting of (002) peak from 9.38° to 6.92° confirms the presence of exfoliated *MXene* material. From Figure 22(b) *d*-spacing and c lattice parameter were calculated and obtained from (002) peak, where the *d*-spacing of MAX was 9.43^{-10} and for *MXene* 12.77^{-10} . The calculated C lattice constant for MAX was 18.85-10 and for *MXene* was 25.53-10. The c lattice parameter (LP c) increased from 18.4 Å to 25.5082 Å before and after chemical etching [39]. With a long processing time, Ti_3AlC_2 peaks decreased and *MXene* peaks appeared based on the XRD pattern. Therefore, a conclusion can be drawn from our results that a longer time (48 h), and etching temperature (45°C) are required and are enough for the full exfoliation of Ti_3AlC_2.

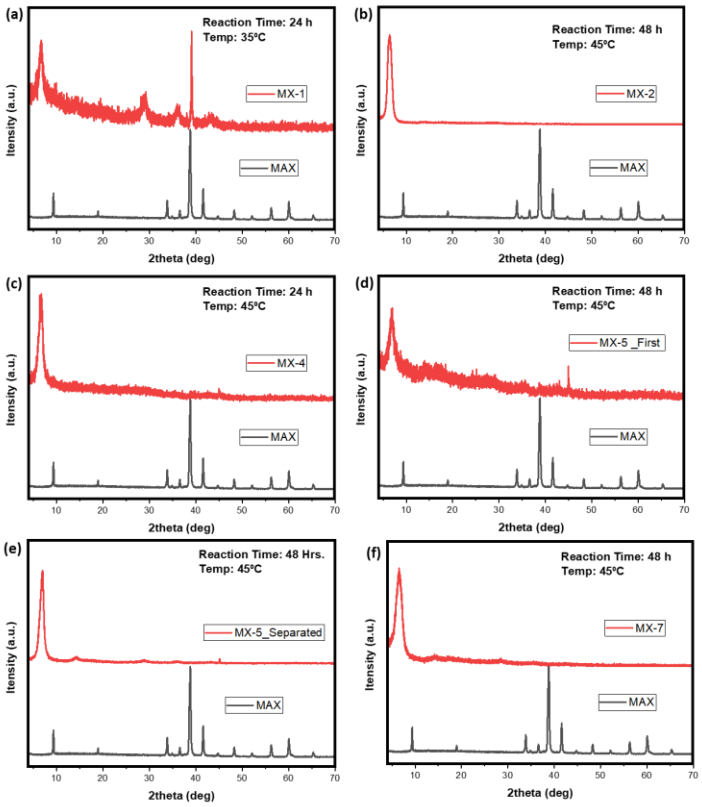

Figure 21. XRD patterns of starting material vs. resulting etched *MXene* at different reaction times and temperature.

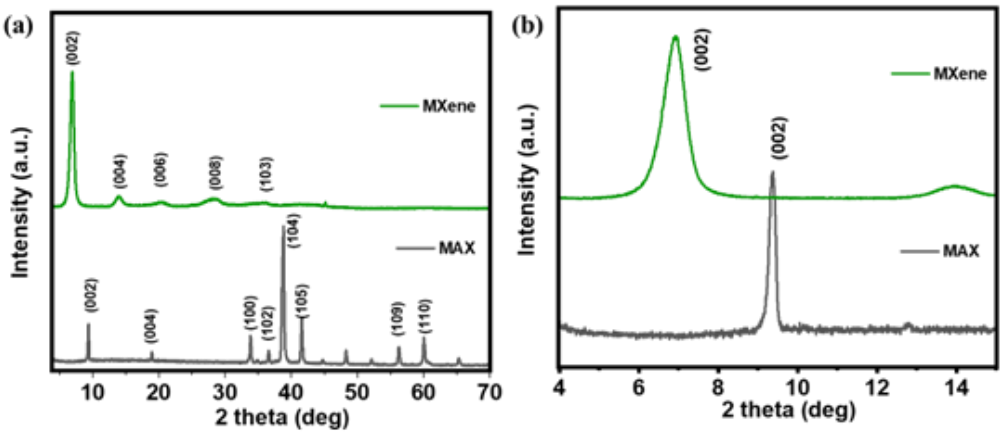

Figure 22. (a) XRD patterns of the starting material (Ti_3AlC_2 powder) vs. resulting $Ti_3C_2T_x$ etched by using LiF and HCl chemical mixtures. (b) Magnified XRD pattern of (002) Plane peak.

4.3 Scanning Electron Microscope (SEM)

Scanning electron microscope is a technique that analyzes the morphological features of exfoliated few-layer *MXene* material. From SEM measurements with Ti_3AlC_2 it tends to exhibit an apparent expansion of closed packing structures while in comparison with etched *MXene* the flake structures tend to be highly unpacked depending on the length and increasing of etching time as well as *MXene* weight percentage. The weight percentage of both the factors and the etching time of Ti_3AlC_2 are essential factors that could determine the formulation of high quality *MXene* material. Furthermore, the $Ti_3C_2T_x$ materials will showcase an accordion like structure. SEM analysis on prepared *MXene* flakes and free-standing film was conducted on Hitachi Scanning Electron Microscope SU8230 model (Tokyo, Japan) with an accelerating voltage of 15 kV.

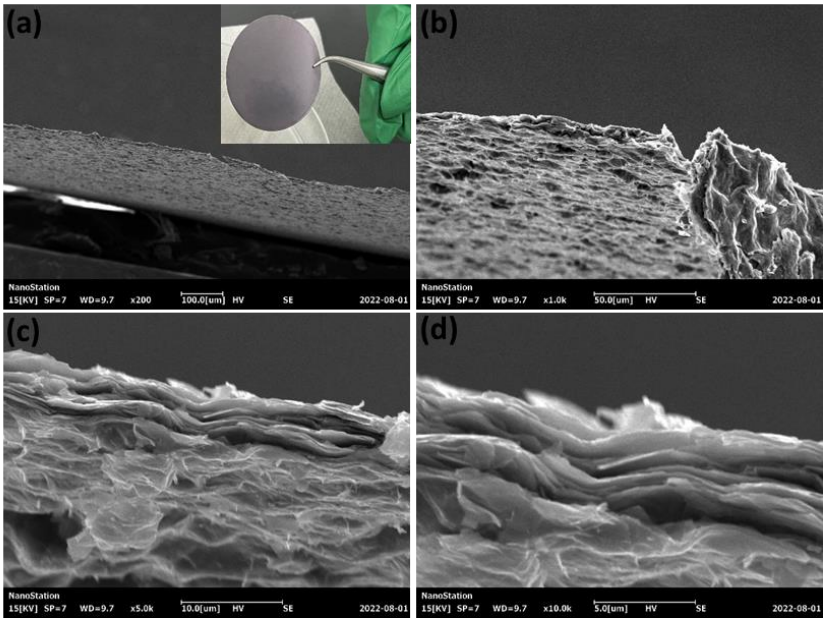

Figure 23. (a-d) SEM visualization of chemically exfoliated $Ti_3C_2T_x$ from MAX etched at 48 hours at 45°C. and (b-d) Cross sectional view of *MXene* free standing film shows layer by layer stacking of *MXene* layers during film formation at different magnification.

The ultrathin sharp edges of the samples shown in Figure 23 confirm the quality of the fabrication procedure. The multiple loosely packed structures and thin sheet layers indicate the higher aluminum removal efficiency, meaning that the *MXene* was effectively etched out from its MAX phase with the removal of the Al layer. The resulting ultrathin sheet layers confirm the quality of the fabrication procedure of $Ti_3C_2T_x$ (*MXene*) that can be acquired via the etching process using hydrofluoric acid and lithium fluoride.

4.4 Transmission Electron Microscopy (TEM)

Transmission electron microscopy is a measurement technique that analyzes layer structures of *MXene* material. TEM is a quantitative method that can determine the particle size, shape, and distribution of a material. The prepared *MXene* materials were diluted with deionized water and then drop casted onto TEM grids and were visualized by transmission electron microscopy (TEM) FEI Tecnai Osiris (JEOL JEM2010) (S)TEM with an accelerating voltage of 200 kV.

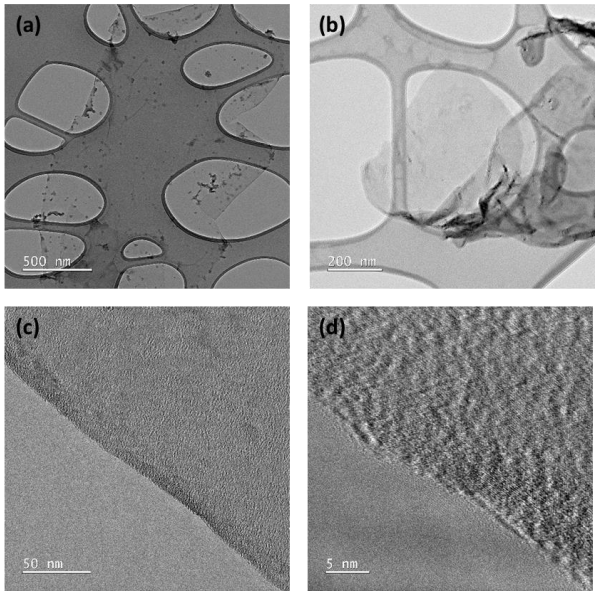

Figure 24. (a and b) TEM characterization image of *MXene* materials under different low magnification. (c and d) magnified TEM images of *MXene* flakes.

Figure 24 shows TEM images of 2D *MXene* samples etched from MAX for 48 h at 45°C. Figure 24(a) showcases typical transmission electron microscope micrographs for individual $Ti_3C_2T_x$ *MXene* flakes with diverse lateral sizes are shown. Most of the lateral dimensions of the flakes generally are in the range of hundreds of nanometers up to several micrometers. It is seen in Figure 24(a) that the $Ti_3C_2T_x$ flakes observed are flat and nearly transparent to electrons under TEM because other sheets are clearly seen below them. It is visible that there are multiple sheets on top of each other and that each of these thin foil layers are where Ti or C layer sheet of one $Ti_3C_2T_x$ is present. Figure 24(c-d) shows TEM image of the sample under a higher magnification where the thickness of a single layer of *MXene* were visible seen. Overall, by adopting suitable etching conditions the high quality $Ti_3C_2T_x$ ultrathin *MXene* can be formed via the MILD etching process using hydrofluoric acid and lithium fluoride.

4.5 Atomic Force Microscopy (AFM)

Atomic force microscopy is a novel technique that is able to image surface roughness, flake size, and flake thicknesses of 2D materials, including those of *MXene* material. Atomic force microscope (AFM) analysis of exfoliated material was administered on (Veeco Multimodal) AFM tool using prepared *MXene* free-standing films and the dispersed flakes. From conducting AFM measurements using a tapping mode configuration, the number of layers in a single flake can be calculated. AFM analysis of exfoliated *MXene* material unveils that most of the flakes have a vertical distance (i.e., height) less than 10 nm and have a lateral size of 1-3 micron. Figure 25(a) exhibits an individual *MXene* sheet from AFM measurement. Figure 25(b) displays thickness distribution chart of several measured *MXene* flakes. As seen in Figure 25(b) from these measurements most of $Ti_3C_2T_x$ flakes range from roughly 10-14 nm thick in thickness.

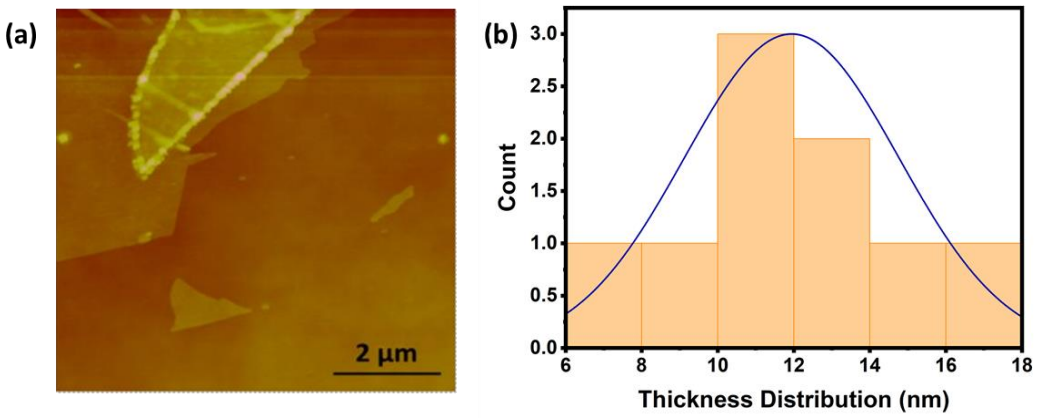

Figure 25. (a) AFM image of *MXene* material flake, the thickness of most flakes is less than 10 nm (less than 10 layers). (b) Distribution chart of $Ti_3C_2T_x$ flakes thickness taken from AFM.

AFM analysis of exfoliated material helped to determine the lateral dimensions as well as flake thickness. Representative AFM images and corresponding histogram of flake length, area, volume, and thickness are shown in Figure 25. From AFM it unveils that most of the flakes have a vertical distance size less than 10 nm and have a lateral size in the range between 1 to 3 µm, which corresponds to that less than 10 *MXene* layers are present.

4.6 X-ray Photoelectron Spectroscopy (XPS)

X-ray photoelectron spectroscopy analysis is a technique that measures and analyzes chemically treated MAX-phase materials and their corresponding *MXene* materials. This technique evaluates the chemical environment of several atoms that are present in the material and typically displays a survey spectrum with individual elemental peaks such as titanium, carbon, oxygen, and fluorine in case of $Ti_3C_2T_x$ *MXene* and additionally of aluminum in case of the MAX phase. Overall, results from XPS analysis provide the evolution of the exfoliation of the $Ti_3C_2T_x$ *MXene* layered structure as well as surface active groups. The X-ray photoelectron spectroscopy was

conducted on Thermo Scientific K-alpha X-ray photoelectron spectroscopy (XPS) using Aluminum X-ray source.

To investigate the elemental composition of the surface functional groups of the chemically etched *MXene* the use of X-Ray photoelectron spectroscopy (XPS) characterization was conducted on the prepared $Ti_3C_2T_x$ samples directly after synthesis. X-ray photoelectron spectroscopy (XPS), also known as electron spectroscopy for chemical analysis (ESCA), is a technique for analyzing the surface chemistry of a material. XPS can measure the elemental composition, empirical formula, chemical state, and electronic state of the elements within a material [43].

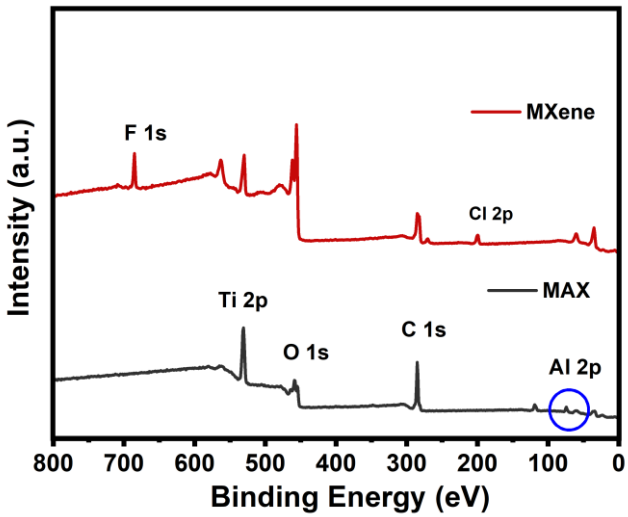

Figure 26. XPS spectra of titanium aluminum carbide MAX and chemically exfoliated titanium carbide *MXene*.

Figure 26 shows the full XPS survey of the synthesized *MXene* with F 1s, Ti 2p, O 1s, Cl 2p, and Al 2p peaks identified with their relative energy values in the binding energy spectrum. The full XPS spectrum confirms the removal of the intermediate aluminum layer and the creation of a *MXene* layered structure with the disappearance of the Al 2p peak in the *MXene* survey as

shown in Figure 26. However, some of the peaks can be influenced from the etching process where lithium fluoride was used and washing cycles to be further optimized where the fluoride peaks can be dramatically seen and observed (Figure 27 i).

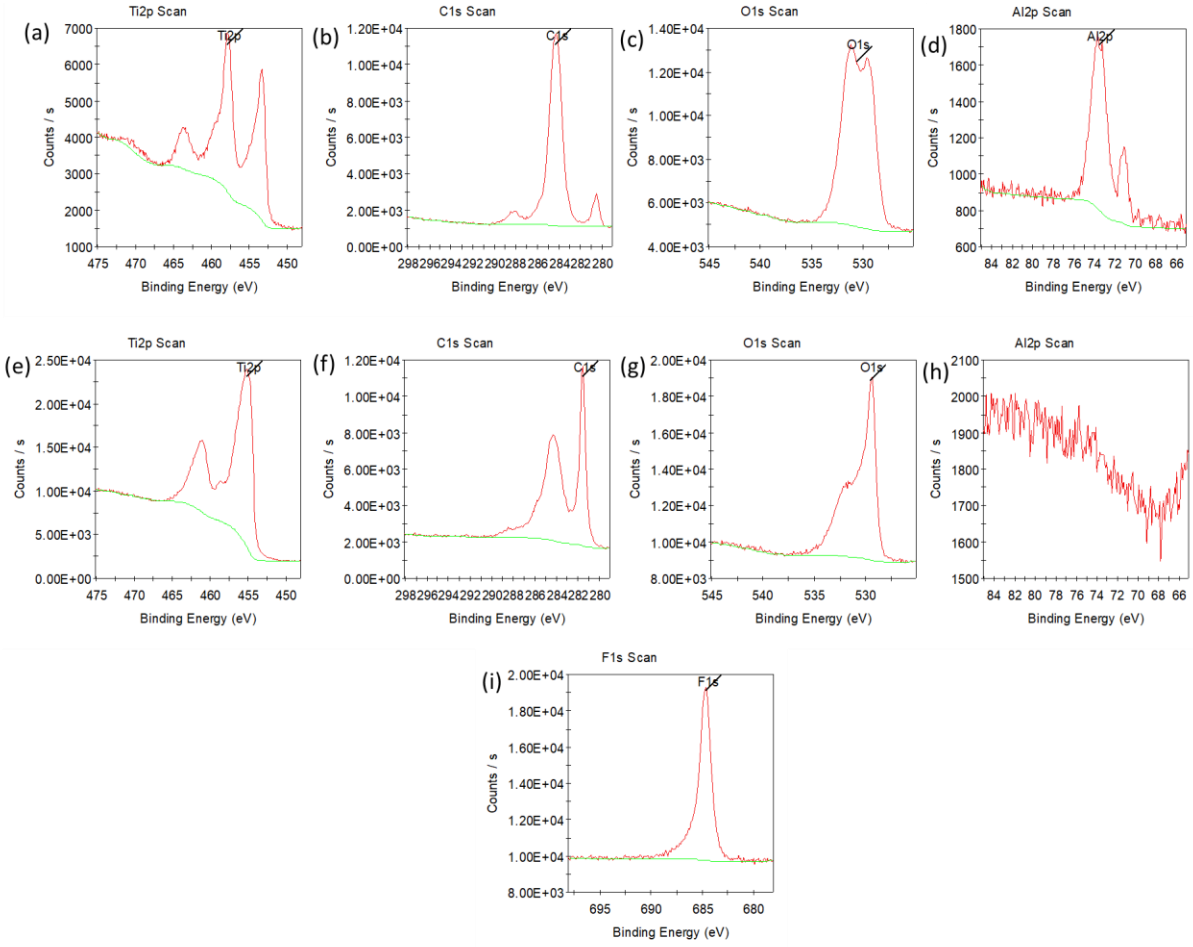

Figure 27. (a-i) XPS spectra of Ti 2p, C 1s, O 1s, Al 2p, and F 1s deconvoluted peak fittings of *MXene*.

The deconvoluted XPS peak fittings originating from the presence of underlying chemical species are exhibited in Figure 27 (a-i). The Ti 2p spectrum has two peaks around 462 eV and 455 eV. The higher BE of Ti 2p (455.50 eV) of Ti_3AlC_2 is attributed to the replacement of Al into electronegative surface tail groups (-O, -OH and -F) on the surface and edges of $Ti_3C_2T_x$. Corresponding to the C 1s spectra the peaks were fitted at 283 eV and 285 eV. Furthermore, for O

1s region the peaks were fitted at 529 eV and 533 eV. In the case of the Al 2p spectra the XPS peaks were fitted at 71 eV and 73 eV. The fitted components for Al 2p observed at 71 eV and 73 eV related to AlF_x and Al_2O_3 were greatly reduced, which indicated that the majority of Al was removed from the MAX phase after etching treatment. Lastly, the F 1s spectra were fitted at 285 eV. Overall, the results of the XPS analysis confirm the development of the exfoliation of Ti_3C_2Tx *MXene* layered structure and their surface-active groups from the MAX phase obtained through MILD chemical etching.

4.7 Raman Spectroscopy

Raman spectroscopy is a fast, noninvasive, and sensitive spectroscopic measurement method that is able to record spectra even from single flake of many 2D materials. Raman spectroscopy, which measures lattice vibrations, can provide information about bonding in the *MXene* structure. From Raman spectra of $Ti_3C_2T_x$ not only the composition and surface groups are studied but also the intercalated species and stacking order of $Ti_3C_2T_x$ could be extracted. In our case, the prepared *MXene* free-standing film was used to conduct Raman spectroscopy measurements. The sample was exposed to incident laser excitation for an exposure time of 100 seconds, in the measurement window of 100-1800 cm^{-1}, with laser relative power/intensity of 5 percent and accumulation time of 1.

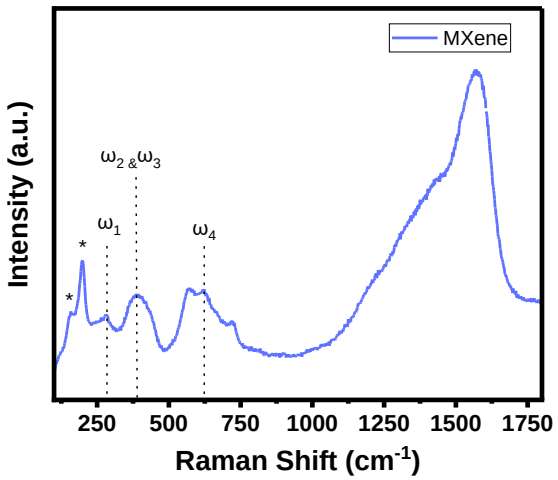

Figure 28. Raman spectrum obtained from a Ti_3C_2Tx film synthesized by MILD etching method. Peaks marked with * are assigned to the out of plane vibrations of Ti and C atoms.

Raman spectroscopy is one of the most useful tools for the analysis of two-dimensional (2D) materials. *MXene*s are a very large family of 2D transition metal carbides and nitrides; however, there have been just a few Raman studies of materials from this family [38]. As shown in Figure 28 the Raman spectrum displays the signature of $Ti_3C_2T_x$ in the wavenumber ranges from 100-1800 cm^{-1}. The peaks labelled as ω1, ω2 & ω3, ω4 in spectrum were located around 282, 386, and 620 cm^{-1} respectively. These peaks are key features of Ti3AlC2, and matched well with those reported in the literature, attributed to shear and longitudinal oscillations of Ti and the Al atoms [45].

4.8 Conductivity using Four-Probe

The most common way of measuring the resistivity of an electronic material is by using a four-point collinear probe. This technique involves four equally spaced electrical probes that encounter a material of an unknown resistivity. Four-probe electrical conductivity (or, resistivity) measurements were studied with the prepared *MXene* free-standing films. Conductivity depends on the source of MAX powder, etching conditions, and the quality in the overall process of

synthesizing *MXene*, for instance oxidation and defects. The measured thickness of the prepared *MXene* free-standing film is 4.26µm and the extracted conductivity is found to be 12139.01736 S cm^{-1}. Furthermore, this closely corresponds to the reported electrical conductivity of synthesized $Ti_3C_2T_x$ *MXene*s etched using with HCl-LiF etching and delamination route (~ 7900 ± 620 S cm^{-1}) [43].

4.9 Fabrication of Voltera printed *MXene* sensor electrodes

The demand for rapid prototyping is evolving and incorporating additive free ink is a promising method for the scalable production of devices that are cost efficient, environmentally friendly, agile fabrication, and minimal waste of the materials, compared with traditional methods such as screen printing and etching processes. For instance, the MILD method avoids the usage of toxic etchants such as HF. For sensing applications, here the printed electrochemical sensor was fabricated in the following steps. First, flexible polyimide sheets (purchased from 3M) were cleaned with acetone, methanol, and isopropanol and bath sonicated for five minutes each cycle. Second, the substrate was dried using a nitrogen gun. Third, the electrode design was created in Voltera V- One two-dimensional design software KidCad. The *MXene* ink was filled inside the Voltera conductive ink dispenser, which was attached to the Voltera printer. The design created on KidCad was transferred patterned onto the cleaned polyimide sheet. Silver conductive ink was then applied at the top of the electrode stem to act as a contact and clear nail polish was painted onto the rest of the electrode stem. Finally, the fabricated electrodes were then air-dried for more than 24 h as shown in Figure 29.

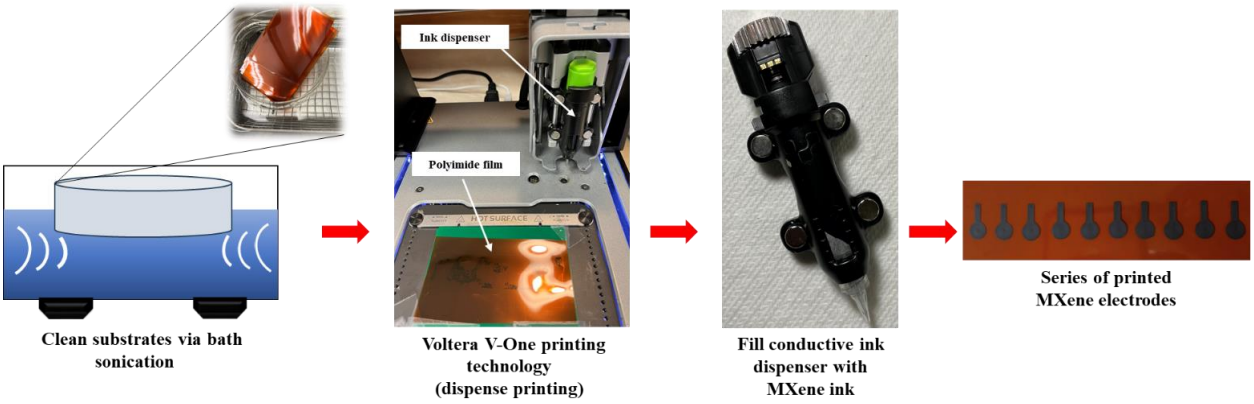

Figure 29. Schematic of water based *MXene* ink printed electrochemical electrodes fabrication via dispense printing process.

4.10 Optimization of the Voltera printed sensors

To further improve the performance of *MXene* sensing applications, chitosan acted as a binder and was drop casted on top of the working area of the printed electrode to help analyze and control the current performance of the sensor. Chitosan binder was formulated by taking 100 µL of acetic acid and mixing it with 10 mL of distilled water. Then, 0.1 g of chitosan was measured and added into the aqueous solution to achieve 0.1 g of solution. The mixture was then kept for stirring for 3 hr at 1500 rpm at room temperature or stirred until the solution was clear. Finally, 100 µL of the achieved 0.1 g chitosan solution was drop casted on top of the printed *MXene* electrode with optimized *MXene* ink and air dried for 24 h as shown in Figure 30b. Figure 30a highlights how three droplet sizes of produced chitosan binder onto the substrate of interest were studied. This specific study provided the results of how much chitosan will fully cover the working area of the optimized printed *MXene* sensor, where 100 µL of chitosan provided optimal coverage of the printed *MXene* electrode.

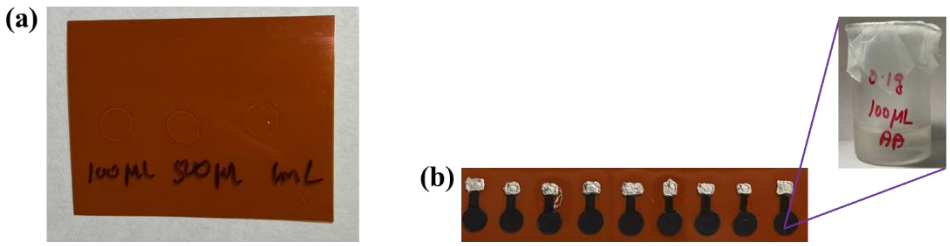

Figure 30. (a) 100 µL, 500 µL, and 1 mL of chitosan binder drop casted onto polyimide substrate (b) optimized fabricated dispense printed *MXene* electrodes with 100 µL of chitosan dropped cast onto the working area.

4.11 Electrochemical sensing

Investigation of inherent electrochemistry of pure GCE and *MXene*/GCE electrode under anodic and cathodic cyclic voltammetry (CV) in the potential window of –1.4 to +0.4 V (electrolyte: pH 5 PBS and concentrated HCl solution, all the potentials stated are measured versus an Ag/AgCl reference electrode). Three consecutive scans were recorded for each pure GCE and *MXene*/GCE electrode. Figure 31a shows the comparison of CV curve of pure GCE and *MXene*/GCE electrode measured under 0.1 M PBS electrolyte. As supported from Figure 31a, the *MXene* coated GCE shows higher current compared with GCE due to high electrical conductivity of *MXene*.

Furthermore, similar CV experimental conditions were done for 100 µM of 4-Nitrophenol at different scan rates, where the scan rates ranged from 10mV/s to 200mV/s as shown in Figure 31b. Figure 31c-d highlights the plotted linear regression fitting of reduction and oxidation peak current against scan rate, it shows the comparison of peak current fitting as well as the square root of the scan rate of voltametric cycling operation. Results indicate that the cathodic current sensed by *MXene*/GCE is an oxidation peak (R^2 = 0.9991) and reduction peak (R^2 = 0.9967).

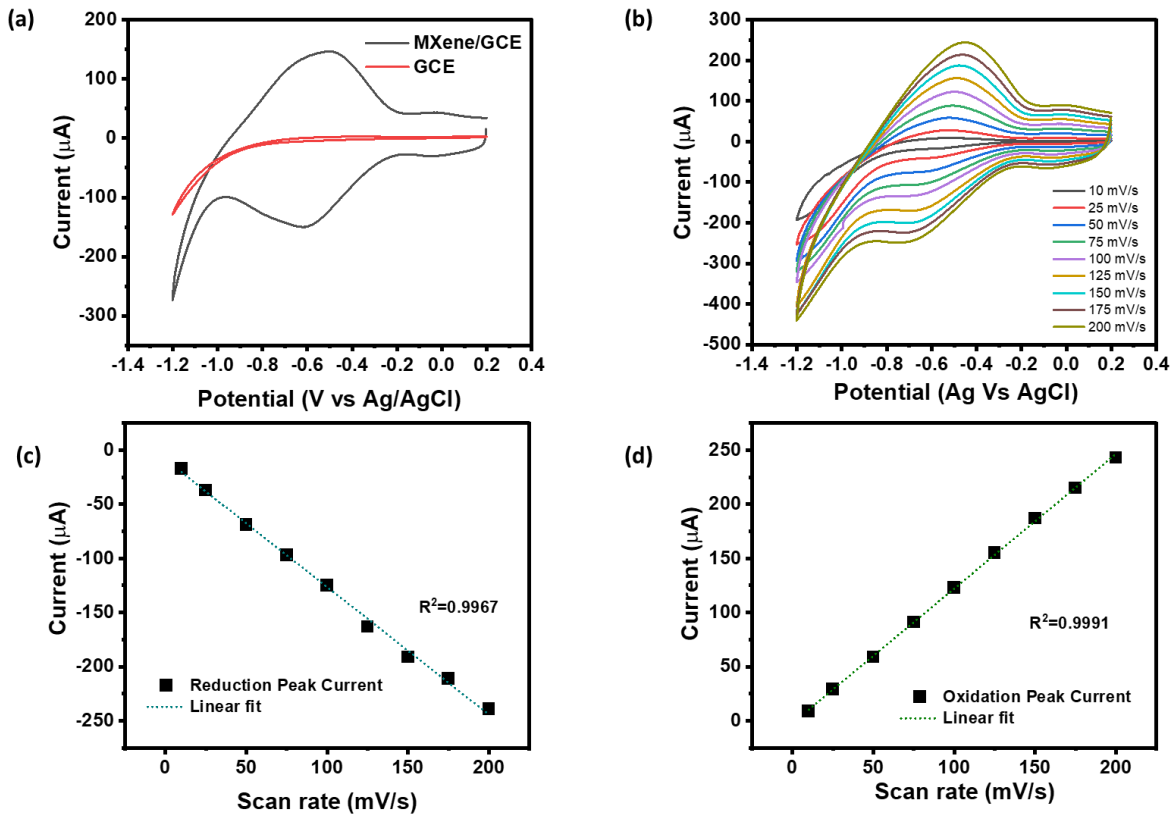

Figure 31. (a) cyclic voltammetry of GCE and *MXene*/GCE electrode measured at 100 mV/s (0.1 M PBS and pH 5) (b) cyclic voltammetry graph with 100 µM of 4-Nitrophenol at different scan rates from 10mV/s to 200mV/s (c-d) linear regression fitting of reduction and oxidation peak current against scan rate.

4.12 Electrochemical detection of 4-Nitrophenol

The analysis of different 4-Nitrophenol concentrations, including the detection limit using *MXene*/GCE was studied by the technique differential pulse voltammetry (DPV). Figure 32a highlights the DPV response of the electrochemical reduction of 4-NP using *MXene*/GCE electrode in 0.1 M PBS (pH 5). Results show that the DPV peak decreases gradually upon continuous addition of 4-NP. In addition, Figure 32b displays the linear regression analysis of the

subject 4-NP concentrations that fit with the respective peak current values. The resulting sensing regimes for 4-Np had an R^2 of 0.99025.

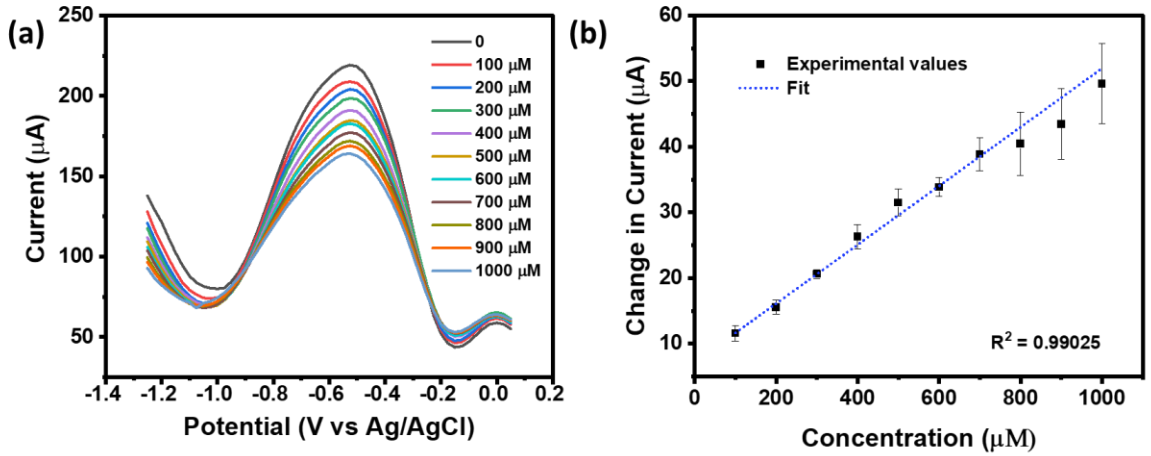

Figure 32. (a) Differential pulse voltammetry curves of 6 µL drop casted *MXene* ink (concentration 0.5 mg/mL) onto GCE surface for different concentrations of 4-NP from 100 µM to 1000 µM measured at 100 mV/s (b) consequent calibration plot between reduction of DPV peak current reading and known concentrations of 4-NP with a linear regression analysis fit.

Finally, the electrochemical measurements of the optimized printed *MXene* sensor, mentioned above with 100 µL of chitosan binder, were performed in a standard electrochemical cell with 0.1 M of PBS and 150 µL of HCl acting as the electrolyte solution. Figure 33 presents the cyclic voltammetry (CV) test of the sensor at a scan rate of 100 mV/s for 3 cycles. The CV test was conducted to analyze the electrochemical activity of chitosan functionalized printed *MXene* electrode toward different concentrations of 4-NP. As seen in Figure 33, the oxidation and reduction peaks were obtained with minimal changes in their corresponding potential values compared to those obtained in *MXene*/GCE electrodes. Electrochemical analysis gives promising evidence that chemically exfoliated $Ti_3C_2T_x$ through the MILD etching route is a material that provides the electrochemical performances desired for the detection of 4-NP.

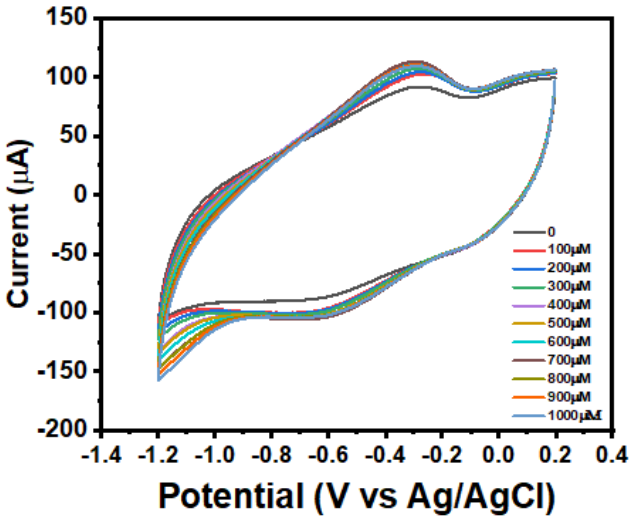

Figure 33. Cyclic voltammetry graph of printed *MXene* electrode with 100µL of 0.1 g of chitosan measured at 100 mV/s for 3 cycles with different concentrations of 4-NP from 100 µM to 1000 µM.

Chapter 5 - Conclusions

5.1 Conclusions

In this present study, the importance of controlled exfoliated *MXene* is emphasized that eliminates the usage of the toxic etchant HF. Subsequently it is shown addressing the efficient dispense printing technology to fabricate and develop *MXene* printed electrochemical sensors that can detect 4-nitrophenol in an acidic environment. This thesis describes a compelling platform for $Ti_3C_2T_x$ ink development for integration in printed devices. By using the minimally intensive layer delamination (MILD) method and dispense printing using Voltera V-One printing technology as a tool for the fabrication as a combination of agile and simplified processes, stable ink formulation, and competitive ink performance is realized. To further improve the performance of *MXene* printed electrodes and sensing applications, a chitosan binder was introduced to optimize the performance of the sensor. Chapter 1 outlines the necessary background of nanomaterials, 0 to two-dimensional (2D) materials, *MXene* and its structure, the properties that *MXene* material encompasses such as its electrical properties, work function, optical properties, magnetic properties, oxidation stability, and the recent progression of *MXene* applications. Chapter 2 outlines the synthesis of *MXene* and the recent progress of $Ti_3C_2T_x$-based conductive inks as well as reported printing methods. Chapter 3 outlines the instruments used to characterize synthesized *MXene* material. Chapter 4 extends the *MXene* ink formulation and the characterization of $Ti_3C_2T_x$ material. In addition, discussion of *MXene* oxidation stability was studied to help improve *MXene* nanosheet dispersion and oxidation stability in different suspensions, which led to surface tension and adhesion considerations. Lastly, the fabrication process of the printed *MXene* sensors were discussed and led to the studies of using the fabricated sensors to perform electrochemical sensing of 4-NP. Overall, this research

showcases promising advancements for printed *MXene* ink in electrochemical sensors for the detection of 4-Nitrophenol in an acidic environment.

To advance the future of *MXene* in this proposed research direction, several key aspects need to be further studied, the related process sciences need to be understood, and the process technologies need to be developed. HF and acid-free synthesis will have a greater promise for both safety as well as industrial compatibility. 4-NP sensing at different pH values necessitates deeper understanding of *MXene*-electrolyte electrochemical interactions and their use will have wider applications. Finally, obtaining an air stable *MXene* for a prolonged time period is the most important requirement for real-world use of *MXene* for its true utilization in technological applications.

References

[1] Ramesh, Kaliat T., and K. T. Ramesh. *Nanomaterials*. Springer US, 2009.

[2] Saleh, Tawfik A. "Nanomaterials: Classification, properties, and environmental toxicities." *Environmental Technology & Innovation* 20 (2020): 101067.

[3] Kahan, Dan M., et al. "Cultural cognition of the risks and benefits of nanotechnology. "*Nature nanotechnology* 4.2 (2009): 87-90.

[4] Yang, Zhoufei, et al. "Carbon nanotube-and graphene-based nanomaterials and applications in high-voltage supercapacitor: A review." *Carbon* 141 (2019): 467-480.

[5] Pomerantseva, Ekaterina, et al. "Energy storage: The future enabled by nanomaterials." *Science* 366.6468 (2019): eaan8285.

[6] Novoselov, Kostya S., et al. "Electric field effect in atomically thin carbon films." *science* 306.5696 (2004): 666-669.

[7] Zhang, Xu, An Chen, and Zhen Zhou. "High-throughput computational screening of layered and two-dimensional materials." *Wiley Interdisciplinary Reviews: Computational Molecular Science* 9.1 (2019): e1385.

[8] Wang, Hao, Patrick Urbankowski, and Yury Gogotsi. "Topochemical synthesis of 2D materials." (2018).

[9] Iqbal, Aamir, et al. "Anomalous absorption of electromagnetic waves by 2D transition metal carbonitride Ti3CNT x (MXene)." *Science* 369.6502 (2020): 446-450.

[10] Naguib, Michael, et al. "Two-dimensional nanocrystals produced by exfoliation of Ti3AlC2." *Advanced materials* 23.37 (2011): 4248-4253.

[11] Tao, Quanzheng, et al. "Atomically layered and ordered rare-earth i-MAX phases: a new class of magnetic quaternary compounds." *Chemistry of Materials* 31.7 (2019): 2476-2485.

[12] Dahlqvist, Martin, et al. "Prediction and synthesis of a family of atomic laminate phases with Kagomé-like and in-plane chemical ordering." *Science advances* 3.7 (2017): e1700642.

[13] Li, Mian, et al. "Element replacement approach by reaction with Lewis acidic molten salts to synthesize nanolaminated MAX phases and MXenes." *Journal of the American Chemical Society* 141.11 (2019): 4730-4737.

[14] Gogotsi, Yury, and Babak Anasori. "The rise of MXenes." *ACS nano* 13.8 (2019): 8491-8494.

[15] Huang, Kai, et al. "Two-dimensional transition metal carbides and nitrides (MXenes) for biomedical applications." *Chemical Society Reviews* 47.14 (2018): 5109-5124.

[16] Zhang, Hua. "Ultrathin two-dimensional nanomaterials." *ACS nano* 9.10 (2015): 9451-9469.

[17] Zhang, Jizhen, et al. "Scalable manufacturing of free-standing, strong Ti3C2Tx MXene films with outstanding conductivity." *Advanced Materials* 32.23 (2020): 2001093.

[18] Alhabeb, Mohamed, et al. "Guidelines for synthesis and processing of two-dimensional titanium carbide (Ti3C2T x MXene)." *Chemistry of Materials* 29.18 (2017): 7633-7644.

[19] Tahini, Hassan A., Xin Tan, and Sean C. Smith. "The origin of low workfunctions in OH terminated MXenes." *Nanoscale* 9.21 (2017): 7016-7020.

[20] Schultz, Thorsten, et al. "Surface termination dependent work function and electronic properties of Ti3C2T x MXene." *Chemistry of Materials* 31.17 (2019): 6590-6597.

[21] Liu, Yuanyue, Hai Xiao, and William A. Goddard III. "Schottky-barrier-free contacts with two-dimensional semiconductors by surface-engineered MXenes." *Journal of the American Chemical Society* 138.49 (2016): 15853-15856.

[22] Zhang, Chuanfang, et al. "Additive-free MXene inks and direct printing of micro-supercapacitors." *Nature communications* 10.1 (2019): 1795.

[23] El-Demellawi, Jehad K., et al. "Tunable Multipolar Surface Plasmons in 2D Ti3C2Tx MXene Flakes." *ACS nano* 12.8 (2018): 8485-8493.

[24] Hu, Lin, Xiaojun Wu, and Jinlong Yang. "Mn 2 C monolayer: a 2D antiferromagnetic metal with high Néel temperature and large spin–orbit coupling." *Nanoscale* 8.26 (2016): 12939-12945.

[25] Yoon, Yeoheung, et al. "Low temperature solution synthesis of reduced two dimensional Ti3C2 MXenes with paramagnetic behaviour." *Nanoscale* 10.47 (2018): 22429-22438.

[26] Tian, Jingjing, et al. "Inorganic halide perovskite solar cells: progress and challenges." *Advanced energy materials* 10.23 (2020): 2000183.

[27] Zhang, Jin, et al. "Defect engineering in atomic-layered graphitic carbon nitride for greatly extended visible-light photocatalytic hydrogen evolution." *ACS applied materials & interfaces* 12.12 (2020): 13805-13812.

[28] Maleski, Kathleen, Vadym N. Mochalin, and Yury Gogotsi. "Dispersions of two dimensional titanium carbide MXene in organic solvents." *Chemistry of Materials* 29.4 (2017): 1632-1640.

[29] Abdolhosseinzadeh, Sina, et al. "Perspectives on solution processing of two-dimensional MXenes." *Materials Today* 48 (2021): 214-240.

[30] Dai, Jie, et al. "Printed gas sensors." *Chemical Society Reviews* 49.6 (2020): 17561789.

[31] Elgrishi, Noémie, et al. "A practical beginner's guide to cyclic voltammetry." *Journal of chemical education* 95.2 (2018): 197-206.

[32] Naguib, Michael, et al. "Two-dimensional materials: 25th anniversary article: MXenes: a new family of two-dimensional materials (Adv. Mater. 7/2014)." *Advanced Materials* 26.7 (2014): 982-982.

[33] Cullity, Bernard Dennis. *Elements of X-ray Diffraction*. Addison-Wesley Publishing, 1956.

[34] Scientific, Thermo Fisher. "Principles of Scanning Electron Microscopy." *Electron matter interactions: the different types of signals which are generated*.

[35] Eaton, Peter, and Paul West. *Atomic force microscopy*. Oxford university press, 2010.

[36] Scientific, Thermo Fisher. "Seeing with Electrons." The Anatomy of an Electron Microscope.

[37] 2023 Physical Electronics, Inc. (PHI). "XPS / ESCA".

[38] Rajavel, Krishnamoorthy, et al. "Condition optimization for exfoliation of two dimensional titanium carbide (Ti3C2Tx)." *Nanotechnology* 29.9 (2018): 095605.

[39] Chemistry of Materials 2020 32 (8), 3480-Sarycheva, Asia, and Yury Gogotsi. "Raman spectroscopy analysis of the structure and surface chemistry of Ti3C2T x MXene." Chemistry of Materials 32.8 (2020): 3480-3488.

[40] Mulvaney, Shawn P., and Christine D. Keating. "Raman spectroscopy." Analytical Chemistry 72.12 (2000): 145-158.

[41] Zrimsek, Alyssa B., et al. "Single-molecule chemistry with surface-and tip-enhanced Raman spectroscopy." *Chemical reviews* 117.11 (2017): 7583-7613.

[42] Thakur, Anupma, et al. "Step-by-Step Guide for Synthesis and Delamination of Ti3C2Tx *MXene*." *Small Methods* (2023): 2300030.

[43] Guo, Tiezhu, et al. "Rational Design of Ti3C2T x MXene Inks for Conductive, Transparent Films." *ACS nano* 17.4 (2023): 3737-3749.

[44] Natu, Varun, et al. "A critical analysis of the X-ray photoelectron spectra of Ti3C2Tz MXenes." *Matter* 4.4 (2021): 1224-1251.

[45] Spanier, Jonathan E., et al. "Vibrational behavior of the M n+ 1 A X n phases from first-order Raman scattering (M= Ti, V, Cr, A= Si, X= C, N)." *Physical Review B* 71.1 (2005): 012103.